https://doi.org/10.5194/acp-2020-344
Preprint. Discussion started: 6 May 2020

Atmospheric Chemistry and Physics Discussions

Evaluating the simulated radiative forcings, aerosol properties and stratospheric warmings from the 1963 Agung, 1982 El Chichón and 1991 Mt Pinatubo volcanic aerosol clouds

Sandip S. Dhomse[1,2], Graham W. Mann[1,3], Juan Carlos Antuña Marrero[4], Sarah E. Shallcross[1], Martyn P. Chipperfield[1,2], Ken S. Carslaw[1], Lauren Marshall[1,5], Nathan Luke Abraham[5,6], and Colin E. Johnson[3,7]

[1]School of Earth and Environment, University of Leeds, Leeds, UK
[2]National Centre for Earth Observation, University of Leeds, Leeds, UK
[3]National Centre for Atmospheric Science (NCAS-Climate), University of Leeds, UK
[4]Department of Theoretical Physics, Atomic and Optics, University of Valladolid, Valladolid, Spain
[5]Department of Chemistry, University of Cambridge, Cambridge
[6]National Centre for Atmospheric Science, University of Cambridge, UK
[7]Met Office Hadley Centre, Exeter, UK

Correspondence: Sandip Dhomse (s.s.dhomse@leeds.ac.uk), Graham Mann (g.w.mann@leeds.ac.uk)

Abstract. Accurate quantification of the effects of volcanic eruptions on climate is a key requirement for better attribution of anthropogenic climate change. Here we use the UM-UKCA composition-climate model to simulate the global dispersion of the volcanic aerofsol clouds from the three largest eruptions of the 20th century: 1963 Agung, 1982 El Chichón and 1991 Pinatubo. The model has interactive stratospheric chemistry and aerosol microphysics, with coupled aerosol-radiation interactions for realistic composition-dynamics feedbacks. Our simulations align with the design of the Interactive Stratospheric Aerosol Model Intercomparison (ISA-MIP) "Historical Eruption SO_2 Emissions Assessment". For each eruption, we perform 3-member ensemble model experiments with upper, mid-point and lower estimates for SO_2 emission, each initialised to a meteorological state to match the observed phase of the quasi-biennial oscillation (QBO) at the times of the eruptions. We assess how each eruption's emitted SO_2 evolves into a tropical reservoir of volcanic aerosol and analyse the subsequent dispersion to mid-latitudes.

We compare the simulations to the three volcanic forcing datasets used in historical integrations for the two most recent Coupled Model Intercomparison Project (CMIP) assessments: the Global Space-based Stratospheric Aerosol Climatology (GloSSAC) for CMIP6, and the Sato et al. (1993) and Ammann et al. (2003) datasets used in CMIP5. We also assess the vertical extent of the volcanic aerosol clouds by comparing simulated extinction to Stratospheric Aerosol and Gas Experiment II (SAGE II) v7.0 satellite aerosol data (1985-1995) for Pinatubo and El Chichón, and to 1964-65 northern hemisphere ground-based lidar measurements for Agung. As an independent test for the simulated volcanic forcing after Pinatubo, we also compare to the shortwave (SW) and longwave (LW) Top-of-the-Atmosphere flux anomalies measured by the Earth Radiation Budget Experiment (ERBE) satellite instrument.

For the Pinatubo simulations, an injection of 10 to 14 Tg SO_2 gives the best match to the High Resolution Infrared Sounder (HIRS) satellite-derived global stratospheric sulphur burden, with good agreement also to SAGE II mid-visible and near-

https://doi.org/10.5194/acp-2020-344
Preprint. Discussion started: 6 May 2020


Atmospheric Chemistry and Physics Discussions

infrared extinction measurements. This 10-14 Tg range of emission also generates a heating of the tropical stratosphere that is comparable with the temperature anomaly seen in the ERA-Interim reanalyses. For El Chichon the simulations with 5 Tg and 7 Tg SO2 emission give best agreement with the observations. However, these runs predict a much deeper volcanic cloud than present in the CMIP6 data, with much higher aerosol extinction than the GloSSAC data up to October 1984, but better agreement during the later SAGE II period. For 1963 Agung, the 9 Tg simulation compares best to the forcing datasets with the model capturing the lidar-observed signature of peak extinction descending from 20 km in 1964 to 16 km in 1965.

Overall, our results indicate that the downward adjustment to previous SO_2 emission estimates for Pinatubo as suggested by several interactive modelling studies is also needed for the Agung and El Chichón aerosol clouds. This strengthens the hypothesis that interactive stratospheric aerosol models may be missing an important removal or redistribution process (e.g. effects of co-emitted ash) which changes how the tropical reservoir of volcanic aerosol evolves in the initial months after an eruption. Our analysis identifies potentially important inhomogeneities in the CMIP6 dataset for all three periods that are hard to reconcile with variations predicted by the interactive stratospheric aerosol model. We also highlight large differences between the CMIP5 and CMIP6 volcanic aerosol datasets for the Agung and El Chichón periods. Future research should aim to reduce this uncertainty by reconciling the datasets with additional stratospheric aerosol observations.

1 Introduction

Quantifying the effects of volcanic eruptions on the climate system is challenging due to significant and complex coupling between various atmospheric processes (Cadle and Grams, 1975; Turco et al., 1982; Robock, 2000). Major volcanic eruptions directly inject large amounts of SO_2 into the stratosphere, leading to abrupt enhancement of the stratospheric aerosol layer. The volcanic aerosol cloud then causes a range of other composition responses, which together with the direct aerosol effects, initiates a complex system of radiative, dynamical and chemical interactions. The principal effect of the volcanic aerosol cloud is to greatly increase backscatter of incoming solar radiation, thereby cooling the Earth's surface. As aerosol particles grow larger, they also absorb outgoing longwave (LW) radiation, which offsets some of the shortwave (SW) cooling, also warming the lower stratosphere (e.g. Angell, 1997a; Free et al., 2009). This aerosol-induced stratospheric heating tends to occur within the tropical reservoir of volcanic aerosol, which then enhances upwelling in the lowermost tropical stratosphere. Also, tropical warming alters the tropics-to-pole temperature gradient in the stratosphere, which in turn can modify the vertical propagation (and breaking) of the large planetary and synoptic-scale waves that drive the stratospheric Brewer-Dobson circulation (e.g. Poberaj et al., 2011; Bittner et al., 2016), with additional ozone changes caused by enhanced upwelling (e.g. Kinne et al., 1992; Dhomse et al., 2015). These indirect (circulation-driven) ozone changes also combine with chemical ozone loss from the increased aerosol surface area available for heterogeneous chemistry (e.g. Prather, 1992; Solomon, 1999), and from photochemical ozone changes (e.g. Bekki et al., 1993).

Tropical eruptions that inject SO_2 directly into the stratosphere cause relatively prolonged surface cooling as this region is the long-lived reservoir for the volcanic aerosol (Dyer, 1974) that forms within the tropical pipe region (Plumb, 1996). At the edge of the tropical pipe, strong meridional gradients in wind shear reduce tropics-to-mid-high-latitude transport and subse-

https://doi.org/10.5194/acp-2020-344
Preprint. Discussion started: 6 May 2020


Atmospheric Chemistry and Physics Discussions

quent removal via stratosphere-troposphere exchange (STE) (Holton et al., 1995). The intensity of incoming solar radiation maximises at low latitudes, hence a tropical volcanic aerosol increases also has greatest solar dimming efficacy. The three largest tropical eruptions over the past century are Mt. Agung (March 1963), El Chichón (April 1982) and Mt. Pinatubo (June 1991). The extents to which these eruptions cool the Northern and Southern Hemispheres differ substantially depending on the dispersion pathways of these volcanic aerosol clouds from the tropical reservoir. For El Chichón and Agung, the volcanic aerosol dispersed mostly to the hemisphere of the volcano (e.g. Dyer, 1970; McCormick and Swissler, 1983), whereas for Pinatubo the cloud dispersed to both hemispheres (e.g. Trepte et al., 1993).

Major eruptions are known to cause dominant signatures within decadal surface temperature trends (e.g. Santer et al., 2001, 2014). However, the uncertainty within volcanic forcings such as Agung has only recently become recognised (Marotzke and Forster, 2015). Even with the greater amount of observational data after the most recent major eruption (Pinatubo), the magnitude of the peak stratospheric aerosol optical depth (AOD) remains highly uncertain from 0.3 - 0.45 (e.g. Russell et al., 1996). Global tropospheric cooling estimates from Pinatubo are even more uncertain, ranging from 0.2 K - 0.5 K (Soden et al., 2002; Canty et al., 2013; Folland et al., 2018). The modern satellite era has provided a wealth of information about the progression of volcanic aerosol clouds, but space-borne remote sensing measurements can sometimes have significant uncertainties. Limb-sounding satellite instruments, such as the Stratospheric Aerosol and Gas Experiment (SAGE) and Microwave Limb Sounder (MLS), have large retrieval errors in the presence of volcanically enhanced aerosol loading. Nadir-sounding satellite measurements such as the Advanced Very High Resolution Radiometer (AVHRR) provide important information for the dispersion of the El Chichon (Robock and Matson, 1983) and Pinatubo (e.g. Long and Stowe, 1994) aerosol clouds, but are not able to determine their vertical distribution.

Another important uncertainty for Pinatubo's effects is the lower stratospheric warming, with observational estimates of this effect in the tropical lower stratosphere after Pinatubo eruption in the range 2 K to 4 K (SPARC, 2010, Chap. 8) The magnitudes of the lower stratospheric warmings for El Chichón and Agung eruptions are even more uncertain (e.g. Free et al., 2009; Driscoll et al., 2012; DallaSanta et al., 2019). Such large uncertainties in stratospheric warming are mostly due to differences in the methods used to attribute the volcanic influence, accounting for the phase progression in the quasi-biennial oscillation (QBO) (Angell, 1997a; Sukhodolov et al., 2018), influences from 11-year solar flux variability, (e.g. Lee and Smith, 2003; Dhomse et al., 2011, 2013). The attribution of volcanically forced warming is also complicated by the inherent coupling with changes in tropical upwelling due volcanic aerosol induced heating (e.g. Young et al., 1994; McCormick et al., 1995; Aquila et al., 2013) and associated circulation-driven chemical changes (e.g. Kinne et al., 1992; Dhomse et al., 2015).

Climate models are important research tools to understand past climate change and attribute the impacts of individual external forcings within observed temperature trends. All climate models include interactive aerosol modules for tropospheric aerosol radiative effects, yet very few use these schemes for volcanic forcings. Instead, Coupled Model Intercomparison Project (CMIP) historical integrations with climate models use prescribed volcanic aerosol datasets to mimic effects of the forcings from past eruptions. In CMIP5, most climate models used the NASA Goddard Institute for Space Studies (GISS) volcanic forcing dataset (Sato et al., 1993, hereafter, Sato data), constructed from an extensive synthesis of observational data, originally for 1850-1990, that is often updated to include later eruptions (see https://data.giss.nasa.gov/modelforce/strataer). The Sato dataset

https://doi.org/10.5194/acp-2020-344
Preprint. Discussion started: 6 May 2020


Atmospheric Chemistry and Physics Discussions

consists of zonal-mean stratospheric AOD at 550 nm ($sAOD_{550}$) and column effective radius (Reff). The CMIP5 modelling groups used different approaches to apply this across the spectral wavebands of their model's radiative transfer module and to redistribute the total optical thickness into their model vertical levels (e.g. Driscoll et al., 2012).

Stenchikov et al. (1998) also constructed a forcing dataset for Pinatubo that included the variation in the forcings across wavebands in the SW and LW, combining SAGE II and Stratospheric Aerosol Measurement (SAM) II (McCormick, 1987) aerosol extinctions, as well as data from the Improved Stratospheric and Mesospheric Sounder (ISAMS) (Lambert et al., 1993; Grainger et al., 1993; Lambert et al., 1997), the Cryogenic Limb Array Etalon Spectrometer (CLAES) (Roche et al., 1993), AVHRR, lidar and balloon observations.

Since then, a large number of chemistry-climate models (CCMs) have been developed, and applied to improve our understanding of past stratospheric change. Several co-ordinated hindcast integrations with the CCMs were designed and carried out via activities such as CCMVal (Eyring et al., 2005, 2008; Morgenstern et al., 2010) and CCMI (Eyring et al., 2013; Morgenstern et al., 2017), with each of the models using different methods to include stratospheric heating from volcanic aerosol clouds, so as to represent volcanically-forced changes in stratospheric trace species. Some CCMs prescribed pre-calculated zonal mean heating rate anomalies (e.g. Schmidt et al., 2006), whilst other derived the heating from prescribed aerosol datasets, either the 2-D GISS $sAOD_{550}$ data set or from 3-D prescribed aerosol surface area density (SAD). SPARC (2010, Chap. 8) presented a detailed analysis of lower stratospheric warming in CCMVal-2 simulations following Pinatubo eruptions, that showed a broad range in the simulated lower stratospheric warming (from 0 to 4 K) with SAD-derived warming tending to over-predict the effect.

Another important volcanic forcing dataset is that from Ammann et al. (2003, hereafter, Ammann data), which was produced via a simple parameterisation for the dispersion of the volcanic aerosol from a specified number of major tropical eruptions determined by the seasonal cycle in the Brewer Dobson circulation. The peak aerosol optical depth for each eruption was scaled to match estimates of maximum aerosol loading from Stothers (1996); Hofmann and Rosen (1983b); Stenchikov et al. (1998), assuming a fixed particle size distribution (Reff = 0.42 micron).

Recently, Arfeuille et al. (2014) created the most up-to-date volcanic forcing dataset to to enable models to include aerosol-radiation interactions (aerosol optical properties) consistently with the additional heterogenous chemistry occurring on volcanic aerosol particles. This comprises three datasets, two for SW and LW aerosol optical properties, for each model to map the aerosol onto the wavebands in the radiative transfer module of the host climate model (see Luo, 2016). For the heterogeneous chemistry, a third dataset of SAD was provided, the original version known as the 4λ dataset. An updated version of this dataset (3λ dataset) was produced specifically for the CMIP6 simulations (see ftp://iacftp.ethz.ch/pub_read/luo/CMIP6/). All three datasets were generated from simulations with a 2-D interactive stratospheric aerosol microphysics model (AER), including 26 separate eruptions for the 1600-2013 time period.

Here we analyse volcanic forcing experiments with the Unified Model – United Kingdom Chemistry and Aerosol (UM-UKCA) composition-climate model, which has interactive stratosphere-troposphere chemistry and aerosol microphysics. The model experiments simulate the volcanic aerosol clouds, and associated radiative forcings, from the three largest tropical eruptions over the past century: Mt. Agung (March 1963), El Chichón (April 1982) and Mt. Pinatubo (June 1991). Aligning with

https://doi.org/10.5194/acp-2020-344
Preprint. Discussion started: 6 May 2020


Atmospheric Chemistry and Physics Discussions

the design of the Interactive Stratospheric Aerosol Model Inter-comparison Project (ISA-MIP) co-ordinated multi-model ''Historical Eruption SO_2 Emissions Assessment" (Timmreck et al., 2018), we have carried out 3-member ensembles of simulations with each of upper, low and mid-point best estimates for SO_2 injection for each eruption. Simulated aerosol properties of the volcanic aerosol plume are compared to range of observation-based datasets.

The UM-UKCA experiments includes the online radiative effects from both tropospheric as well as stratospheric aerosol simulated with same interactive aerosol microphysics module. There several important improvements in aerosol microphysics module since the original Pinatubo analysis presented in Dhomse et al. (2014), that are discussed in Brooke et al. (2017); Marshall et al. (2018, 2019); Yoshioka et al. (2019). Section 3 provides the specifics of the model experiments, with section 4 describing the observational datasets. Model results are given in Section 5. Key findings and conclusions are presented in Section 6.

2 Model Experiments

We use the Release Job 4.0 (RJ4.0) version of the UM-UKCA composition-climate model (Abraham et al., 2012), which couples the Global Atmosphere 4.0 configuration (Walters et al., 2014, GA4) of the UK Met Office Unified Model (UM v8.4) general circulation model with the UK Chemistry and Aerosol chemistry-aerosol sub-model (UKCA). The GA4 atmosphere model has a horizontal resolution of $1.875° \times 1.25°$(N96) with 85 vertical levels from the surface to about 85 km. The RJ4.0 configuration of UM-UKCA adapts GA4 with aerosol radiative effects from the interactive GLOMAP aerosol microphysics scheme and ozone radiative effects from the whole-atmosphere chemistry that is a combination of the detailed stratospheric chemistry and simplified tropospheric chemistry schemes (Morgenstern et al., 2009; O'Connor et al., 2014).

The experiment design is similar to that in Dhomse et al. (2014), but with the volcanic aerosol radiatively coupled to the dynamics, as in Mann et al. (2015), transient atmosphere-only free running simulations. Briefly, the model uses the GLOMAP aerosol microphysics module, the scheme configured to be applied across the troposphere and stratosphere with stratosphere-troposphere chemistry. Greenhouse gases (GHGs) and ozone-depleting substance (ODS) concentrations are from Ref-C1 simulation recommendations in the Chemistry-Climate Model Initiative (CCMI-1; Eyring et al. (2013); Morgenstern et al. (2017)) activity. Simulations are performed in atmosphere-only mode, and we use CMIP6 recommended sea-surface temperatures and sea-ice concentration that are obtained from https://esgf-node.llnl.gov/projects/cmip6/. The main updates since Dhomse et al. (2014) are: i) updated dynamical model (from HadGEM3-A r2.0 to HadGEM3 Global Atmosphere 4.0), hence improved vertical and horizontal resolution (N48L60 vs N96L85), ii) coupling between aerosol and radiation scheme (Mann et al., 2015), iii) additional sulphuric particle formation pathway via heterogeneous nucleation on transported meteoric smoke particle cores (Brooke et al., 2017). The atmosphere-only RJ4.0 UM-UKCA model applied here is the identical model to that applied in Marshall et al. (2018) and Marshall et al. (2019), with the former run in pre-industrial setting for the VolMIP interactive Tambora experiment (see Zanchettin et al., 2016) and the latter in year-2000 timeslice mode for the perturbed injection-source-parameter ensemble analysed there.

https://doi.org/10.5194/acp-2020-344
Preprint. Discussion started: 6 May 2020


Atmospheric Chemistry and Physics Discussions

Prior to each of the eruption experiments, we first ran 20-year time-slice simulations with GHGs and ODSs for the corresponding decade (1960 for Agung, 1980 for El Chichón and 1990 for Pinatubo), to allow enough time for the stratospheric circulation and ozone layer to adjust each composition-climate setting for that time period. Tropospheric aerosol and chemistry (primary and precursor) emissions were also set to interactively simulate the tropospheric aerosol layer and oxidising capacity for the corresponding decade. Discarding the first 10 years as spin-up, we then analysed the QBO behaviour in the second 10 years, selecting initialisation fields from three different model years that then ensure each ensemble member approximately matches the post-eruption QBO state seen in the ERA-interim re-analysis (Dee et al., 2011).

For each eruption then, a total of nine different volcanically-perturbed simulations were performed, three different "approximate QBO progressions" for each SO2 emission amount (see Table 1). The 9 control simulations had identical pre-eruption initial conditions and emissions, except the Pinatubo/El Chichon/Agung SO2 emission was switched off. For simplicity the simulations do not use the simulated aerosol in the calculation of heterogeneous chemistry; the control simulations use climatological SAD values in the stratosphere (mean 1995–2006) while the other simulations use time-varying SAD from Arfeuille et al. (2013).

3 Evaluation Datasets

To provide additional context for the UM-UKCA simulated aerosol properties, we compare primarily to the mid-visible and near-infrared extinction from CMIP6 volcanic forcing data set, obtained from ftp://iacftp.ethz.ch/pub_read/luo/CMIP6/ (last access: January 25, 2020) (Luo, 2016). Aerosol properties are derived using various satellite instruments: SAGE I, Stratospheric Aerosol Measurement (SAM), SAGE II, Halogen Occultation Experiment (HALOE), Optical Spectrograph and InfraRed Imager System (OSIRIS), Cloud-Aerosol Lidar and Infrared Pathfinder Satellite Observation (CALIPSO) and Cryogenic Limb Array Etalon Spectrometer (CLAES) measurements.

For the pre-satellite era (1850–1979), volcanic aerosol properties in CMIP6 data are constructed using results from the AER 2-D aerosol model (Arfeuille et al., 2014), considering injection heights in the literature and from plume-rise model, and from comparing to other forcing datasets, ice core sulphate deposition and ground-based solar radiation measurements within Sato et al. (1993) and Stothers (2001). Although the CMIP6 dataset consists primarily of the three parts explained in Introduction section (waveband-mapped aerosol optical properties in the SW and LW, plus surface area density), additional datasets are also provided, including monthly zonal mean log-normal aerosol size distribution properties such as mean radius, volume density and extinctions at 550 nm. These datasets are provided at 0.5 km vertical resolution between 5 km and 40 km).

For 1979–2016, the CMIP6 dataset is replaced with the most up-to-date the Global Space-based Stratospheric Aerosol Climatology data known as the GloSSAC dataset (https://doi.org/10.5067/GloSSAC-L3-V1.0) described in (Thomason et al., 2018). GloSSAC combines stratospheric aerosol information from several different satellite instruments: SAGE I and II, HALOE, OSIRIS, CALIPSO and CLAES. Measurements from other space instruments and in-situ (ground-based, air and balloon-borne) instruments are also used to fill gaps in the dataset where none of these datasets were able to measure the extent of the volcanic cloud. The v1.1 GloSSAC dataset used here is obtained from the NASA Atmospheric Science Data

https://doi.org/10.5194/acp-2020-344
Preprint. Discussion started: 6 May 2020


Atmospheric Chemistry and Physics Discussions

Center (https://eosweb.larc.nasa.gov/ : last access March 10, 2020). During the El-Chichón period, GloSSAC is largely based on SAGE I (January 1979–November 1981) and SAM II (1978–1993) extinction at 1000 nm, and the 550nm extinction derived from fit to the variation in 550:1020 colour ratio that is derived from SAGE II measurements. One limitation is that the SAM II instrument only measures at high-latitudes. After the El-Chichón eruption (SAGE gap period, April 1982–October 1984) data is primarily constructed based on linearly interpolating between data from lidar measurements from the 5 aircraft missions after El Chichón: July 1982 (13°N to 40°N), October and November 1982 (45°S to 44°N), January and February 1983 (28°N to 80°N), May 1983 (59°S to 70°N), and January 1984 (40°to 68°N). For the Pinatubo period, GloSSAC data follows the method described in SPARC (2006, chapter 2), combining SAGE II, HALOE and CLAES measurements. GloSSAC also utilized backscatter-sonde measurements from Lauder, New Zealand (Rosen et al., 1994), ground-based lidar measurements from Mauna Loa, Hawaii (19.5°N, (Barnes and Hofmann, 1997)) from the NASA Langley lidar at Hampton, USA, and Camaguey, Cuba (23°N, see Antuña, 1996)).

For the Agung aerosol cloud, observational data not readily available to evaluate the vertical extent of the aerosol cloud. Hence we digitised the observations from optical radar at Lexington, Massachusetts (42°44' N, 71°15' W Grams and Fiocco, 1967). These aerosol backscatter observations at 694 nm are converted to extinction at 532nm, as described in supplementary material.

For the stratospheric aerosol optical depth (sAOD) comparison, we use three different observation-based datasets. CMIP6 extinctions at 550nm are integrated for all the levels above the tropopause to calculate $sAOD_{550}$. As mentioned earlier, the most widely used volcanic forcing data is from Sato et al. (1993) and is obtained from https://data.giss.nasa.gov/modelforce/strataer/. Another important $sAOD_{550}$ evaluation dataset is based on a combination of simple representation of the dispersion and an assumption of the size distribution by Ammann et al. (2003), and is obtained via ftp://ftp.ncdc.noaa.gov/pub/data/paleo/climate_forcing/volcanic_aerosols/ammann2003b_volcanics.txt. The lower stratospheric warming following each eruption is estimated by comparing 5-year temperature anomalies from the ERA-Interim reanalysis data (ERA-Int, available from www.ecmwf.int). ERA-int data is available since 1979, hence for the Agung comparison, we use ERA40, an earlier version of ECWMF reanalysis datasets.

4 Results and Discussion

The temporal radiative forcing signature from a major tropical eruption is primarily determined by the evolution of the volcanic aerosol cloud in the stratosphere. An initial ''tropically confined phase" sees zonally-dispersing SO_2 and ash plume transforming to layered aerosol cloud. Meridional transport in the subsequent "dispersion phase" then leads to a hemispheric or global cloud of mainly aqueous sulphuric acid droplets. The efficacy of such volcanic clouds' solar dimming, and the extent of any offset via long-wave aerosol absorption, is strongly linked to how large the sulphuric aerosol particles grow (their size distribution) as this large-scale dispersion progresses (e.g Lacis et al., 1992).

In the following subsections we assess, for each eruption, the simulated volcanic aerosol cloud for the upper, lower and mid-point/best-estimate SO_2 emissions and compare to available observational constraints. Our focus here is primarily on

https://doi.org/10.5194/acp-2020-344
Preprint. Discussion started: 6 May 2020


Atmospheric Chemistry and Physics Discussions

aerosol optical properties, evaluating mid-visible stratospheric AOD, but also aerosol extinction, in both the mid-visible and near-infra-red, to understand how the altitude and vertical extent of the cloud varies for each eruption. In each case, we also compare the lower stratospheric warming with the temperature anomaly from the ERA-Interim/ERA-40 reanalyses.

4.1 Mt. Pinatubo aerosol cloud

In the Pinatubo case, satellite measurements are able to constrain the particle size evolution (in terms of effective radius), and hence here we also compare model-simulated effective radius to that provided with the CMIP6 dataset, which underpins each model's specified multi-wavelength aerosol optical properties. With Pinatubo by far the dominant external forcing in the 1990s, we compare simulated SW and LW forcings to the Earth Radiation Budget Experiment (ERBE) satellite data to gain direct insight into how the different SO_2 emission simulations evolve in terms of top-of-the-atmosphere (TOA) radiative forcings.

Baran and Foot (1994) analysed satellite observations of the Pinatubo aerosol cloud from the High-resolution Infrared Radiation Sounder (HIRS), converting the measured LW aerosol optical properties into a timeseries of global aerosol burden. In Dhomse et al. (2014), we used this observed global burden dataset to evaluate the model's simulated aerosol cloud, translating the peak global burden of 19 to 26 Tg from the HIRS measurements into a 3.7 to 6.7 Tg range for stratospheric sulphur, assuming the particles were 75% by weight aqueous sulphuric acid solution droplets. We identified an important inconsistency in the model's predictions, when also considering satellite observations of volcanic SO_2. The satellite measurements of SO_2 show that 7 to 11.5 Tg of sulphur was present in the stratosphere in the days after the eruption (14 to 23 Tg of SO_2, Guo et al. (2004a)), so only around 50% of the emitted sulphur remained present at peak volcanic aerosol loading. In contrast, the model simulations showed that 90% of the sulphur emitted remained in the volcanic aerosol cloud at its peak global mass burden. This inconsistency was also found in other interactive Pinatubo stratospheric aerosol model studies (Sheng et al., 2015a; Mills et al., 2016), with number of models finding best agreement with observations for 10 to 14 Tg emitted SO_2 (5 to 7 Tg of sulphur), which is less than the lower bound from the TOMS/TOVS measurements. In Dhomse et al. (2014), we suggested the models may be missing some process or influence, which acts to redistribute the sulphur within the volcanic cloud, causing it then to be removed more rapidly.

Figure 1a shows the timeseries of global stratospheric aerosol sulphur burden from current Pinatubo simulations compared to the previous model simulations with 20 and 10 Tg SO_2 injection as presented in Dhomse et al. (2014). The 20, 14 and 10 Tg SO_2 Pinatubo clouds generate peak loadings of 8.3, 5.9 and 4.2 Tg of sulphur, translating into conversion efficiencies of 83, 84 and 84%, respectively. This continuing discrepancy with the satellite-derived 50% conversion efficiency might be due to accommodation onto co-emitted ash particles. Recently we have re-configured the UM-UKCA model to enable new simulations to test this hypothesis (Mann et al., 2019b). We consider the requirement to reduce model emitted SO_2 to be less than that indicated by satellite measurements as an adjustment to compensate for a missing removal/redistribution process in the initial weeks after the eruption.

The simulated Pinatubo global stratospheric sulphur burden in runs **Pin10** and **Pin14** is in good agreement with the HIRS observations, both in terms of predicted peak burden, and the evolution of its removal from the stratosphere. In particular, the model captures a key variation in the HIRS measurements, namely that the removal of stratospheric sulphur was quite slow

https://doi.org/10.5194/acp-2020-344
Preprint. Discussion started: 6 May 2020


Atmospheric Chemistry and Physics Discussions

in the first year after the eruption. The volcanic aerosol cloud retained a steady 4-5 Tg of sulphur for more than 12 months before its removal proceeded at much faster rate in late 1992 and early 1993. The corresponding simulations from Dhomse et al. (2014) (**Pin10** and **Pin20**) show a simpler peak and decay curve, the removal from the stratosphere proceeding much faster and earlier than the HIRS measurements indicate.

As shown in Mann et al. (2015), and other studies (Young et al., 1994; Sukhodolov et al., 2018), when interactive stratospheric aerosol simulations of the Pinatubo cloud include the heating effect from aerosol absorption of outgoing LW radiation (i.e. the radiative coupling of the aerosol to the dynamics), the resulting enhanced tropical upwelling greatly changes the subsequent global dispersion. In Mann et al. (2015), we also showed that this coupling improves the simulated tropical mid-visible and near infra-red extinction compared to the SAGE II measurements. We identified that the SAGE II measurements are consistent with the combined effects of increased upwelling and later sedimentation, highlighting the need to resolve composition-dynamics interactions when interactively simulating such major volcanic aerosol clouds.

Here we show that this effect also leads to a quite different global sulphur burden, with the later dispersion peak in the mid-latitude sulphur becoming a greater contributor. This behaviour is explored further in Figure 1b, where we assess the e-folding timescale for the removal of stratospheric sulphur, derived by applyig least squares regression fit on 7-month running-mean mass burden values (3 monthly means either side). We find that a Pinatubo realisation that injects more sulphur produces a volcanic aerosol cloud that is removed more rapidly, the effect apparent throughout the decay period. The timing of the accelerating removal occurs consistently across the 3 runs with residence times for **Pin10**, **Pin14** and **Pin20** decreasing from 9, 6 and 4 months in May 1992, to minima of 5, 3 and 2 months in February 1993.

Later (in Figure 4) we assess the behaviour of model-predicted effective radius, showing that it continues to increase steadily in the tropics throughout 1992, the maximum particle size at 20 km occurring in January 1993. That the maximum effective radius occurs at exactly the same time as the minimum in e-folding time illustrates the importance for interactive stratospheric aerosol models to represent its increased size, sedimentation of particles proceeding faster as the particles grow larger. One thing to note however, is that although the different volcanic SO_2 amount is emitted at the same altitude, since the runs are free-running, later we show that each different emission amount causes different amounts of heating, the resulting enhancements to tropical upwelling lofting the cloud to different altitudes.

The predicted stratospheric sulphur burdens in **Pin10** and **Pin14** compare well to the observations, suggesting a 10 Tg to 14 Tg SO_2 emission range will produce a volcanic aerosol cloud with realistic volcanic forcing magnitude. The comparison could provide a test for other interactive stratospheric models, to identify a model-specific source parameter calibration. It should be noted that such a reduction in emissions, to values below the SO_2 detected (Guo et al., 2004a), is a model adjustment, likely compensating for a missing sulphur loss/re-distribution process.

We also note some differences in sulphur burden between current and previous (Dhomse et al., 2014) Pinatubo simulations. Firstly, the background burden in run **Pin00** is much lower (0.11 Tg) than previous simulations (0.50 Tg) and now in reasonable agreement with (Hommel et al., 2011; Sheng et al., 2015b; Kremser et al., 2016), or with lower end of the ASAP report (SPARC, 2006) (0.12-0.18 for Laramie OPC balloon soundings and 0.12-0.22 Tg Garmisch lidar measurements respectively; there cited as 0.5-0.7 Tg and 0.5-0.9 Tg mass of 75% weight aqueous sulphuric acid solution, respectively). The main reason for the

https://doi.org/10.5194/acp-2020-344
Preprint. Discussion started: 6 May 2020


Atmospheric Chemistry and Physics Discussions

reduction in simulated quiescent stratospheric sulphur burden, compared to Dhomse et al. (2014), is the influence from meteoric smoke particles (MSP), forming meteoric-sulphuric particles (Murphy et al., 2014). One of the effects from simulating these particles, in addition to homogeneously nucleated pure sulphuric acid particles, is to reduce the sulphur residence time (Mann et al., 2019a). There are also some dynamical differences in the updated simulations here, which use an improved vertical and horizontal resolution model (N96L85 rather than N48L60), that might influence stratosphere-troposphere exchange and stratospheric circulation.

Secondly, we also assess the simulated stratosphere into the 3rd post-eruption year (after June 1993). Although for the first two years, the model's global stratospheric sulphur in the simulations **Pin10** and **Pin14** tracks closely with HIRS estimates (Figure 1a), the satellite-derived S-burden drops off rapidly from about 3 Tg in January 1993 to 0.5 Tg by September 1993. On the other hand, the simulated volcanic aerosol cloud does not disperse down to that value until September 1994. However, this accelerated loss of stratospheric sulphur in the HIRS data seems to be inconsistent with other satellite measurements, for example SAGE II measurements (see Figure 3), as well as OPC measurements (Thomason et al., 1997) and CLAES observations (e.g. Bauman et al., 2003; Luo, 2016). This suggests that latter part of the HIRS data may be inaccurate, though it seems difficult to identify a driving mechanism for this. Each of the model experiments suggest the stratosphere remained moderately enhanced throughout 1993 and 1994.

Figure 2 shows, for each eruption magnitude, the zonal mean ensemble-mean stratospheric AOD at 550 nm ($sAOD_{550}$) from the UM-UKCA Pinatubo simulations (**Pin10**, **Pin14**, **Pin20**), compared to three different volcanic forcing datasets. For this period, the GloSSAC data should be considered the primary one, being based on the latest version of the SAGE II, as an update from the gap-filled dataset from the SPARC ASAP report (SPARC, 2006, Chapter 3).

As in the HIRS sulphur burden comparisons (Figure 1), the **Pin20** simulation, which best matches the satellite-observed SO_2 estimates, strongly overpredicts the stratospheric AOD in the tropics and Northern Hemisphere (NH) mid-latitudes, compared to all three reference datasets. However, whereas the lower emissions runs **Pin10** and **Pin14** both closely track the observed global column sulphur variation, run **Pin10** has best agreement with all three reference datasets for mid-visible sAOD. For this run **Pin14** is high-biased in the tropics and NH mid-latitudes. In the tropics, all three emission-magnitude ensembles are higher than the reference datasets.

Figure 2 illustrates the well-established global dispersion pattern for the Pinatubo aerosol cloud: initially confined to the tropical reservoir region, then dispersing to mid-latitudes, following the seasonal variation in the Brewer-Dobson circulation. The over-prediction in the tropics is a common feature among interactive stratospheric aerosol models. It is noticeable that this over-prediction is worst in the first 6-9 months after the eruption, which could indicate the source of the model's discrepancy. Whereas an overly non-dispersive tropical pipe in the model could be the cause, the timing is potentially more consistent with a missing loss pathway that is most effective in the initial months after the eruption. Co-emitted volcanic ash will also have been present within the tropical reservoir, as seen in the airborne lidar depolarisation measurements in the weeks after the eruption (Winker and Osborn, 1992), and remained present in the lowermost part of the mid-latitude aerosol cloud in both hemispheres (Young et al., 1992; Vaughan et al., 1994). The AOD high bias is consistent with the hypothesis that a substantial proportion of the emitted sulphur may have been removed from the stratosphere by accommodation onto the sedimenting ash. If this

https://doi.org/10.5194/acp-2020-344
Preprint. Discussion started: 6 May 2020


Atmospheric Chemistry and Physics Discussions

mechanism is causing such a vertical re-distribution within the tropical reservoir, it will increase the proportion of Pinatubo sulphur being removed into the troposphere via the rapid isentropic transport that occurred during the initial months in the lowermost stratosphere. Furthermore, stratospheric AOD is not a measure of sulphur, and the variations in sAOD will partly indicate changes in scattering efficiency that result from the gradient in effective radius that is disussed in later section.

The peak mid-visible AOD from AVHRR is higher than the SAGE II gap-filled satellite measurements (Long and Stowe, 1994). For example, as noted in Thomason et al. (2018), the peak mid-visible stratospheric AOD in the AVHHR dataset is around 0.4, compared to 0.22 in GloSSAC. However, other possible model biases cannot be ruled out. One consideration for these free-running simulations, even with each ensemble member initialised to approximate the period's QBO phase, is that nudging towards re-analysis meteorology would give more realistic representation of this initial phase of the plume dispersion (Sukhodolov et al., 2018). We chose to perform free-running simulations to allow the enhanced tropical upwelling resulting from increased LW aerosol-absorptive heating, consistent with the SO_2 emission, known to be a strong influence on the subsequent simulated global dispersion (Young et al., 1994).

In contrast to the tropics and NH mid-latitudes, where run **Pin14** agrees best with the reference datasets, run **Pin20** compares best to the Southern Hemisphere (SH) $sAOD_{550}$ measurements in GLOSSAC. Runs **Pin10** and **Pin14** underestimate the cloud in this region. This difference may be highlighting the requirement for a more accurate simulation of the QBO evolution, likely necessary to capture the Pinatubo cloud's transport to SH mid-latitudes (e.g. Jones et al., 2016; Pitari et al., 2016). One thing to note is that our simulations do not include the source of volcanic aerosol formed from the August 1991 Mount Hudson eruption in Chile. However, measurements from SAGE II (Pitts and Thomason, 1993) and ground-based lidar (Barton et al., 1992) indicate that the Hudson aerosol cloud only reached to around 12 km, with the Pinatubo cloud by far the dominant contributor to SH mid-latitude sAOD.

Overall, the $sAOD_{550}$ comparisons confirm the findings from Figure 1 that for UM-UKCA, consistent with other global microphysics models (Sheng et al., 2015a; Mills et al., 2016), Pinatubo aerosol properties are better simulated (acknowledging the discrepancy in the SH) with a 10 Tg to 14 Tg range in volcanic SO_2 emission.

Although Figure 2 suggests significant differences among the volcanic forcing datasets for the Pinatubo period, the GLOSSAC data is the reference dataset while the 1991-4 period in Sato data is mostly based on an earlier version of the SAGE II data. The GloSSAC data have been compared extensively with lidar measurements (Antuña et al., 2002; Antuña, 2003), and combined for the gap-filled dataset (SPARC, 2006) with improvements in the SAGE II aerosol extinction retrieval algorithm (version 7).

For historical climate integrations in CMIP5, some models used the Sato forcing dataset whilst others used Ammann and their differences affect interpretation of volcanic impacts among the models (Driscoll et al., 2012). For CMIP6, all models have harmonised to use the same forcing dataset, with a dedicated VolMIP analysis to compare the climate response in each model and with the GloSSAC Pinatubo forcing applied to the pre-industrial control (Zanchettin et al., 2016).

After comparing the total sulphur burden and sAOD, Figure 3 shows UM-UKCA simulated mid-visible extinction at 3 different altitudes in the lower stratosphere, to evaluate the simulated vertical extent of the Pinatubo cloud through the global dispersion phase. For the tropics, extinction comparisons are shown at 24 km, 28 km and 32 km, whereas for SH (35°S-

https://doi.org/10.5194/acp-2020-344
Preprint. Discussion started: 6 May 2020


Atmospheric Chemistry and Physics Discussions

60°S) and NH (35°N-60°N) mid-latitudes the chosen levels are 20 km, 24 km and 28 km, to account for the higher tropical tropopause. Simulated extinctions are compared with raw SAGE v7.0 data (Damadeo et al., 2013) as well as the gap-filled GloSSAC product (Thomason et al., 2018) at 525 nm. As discussed previously, extinctions from **Pin14** (and to some extent **Pin10**) show much better agreement with observational data for all three latitude bands. Most importantly, model extinction remain close or slightly lower in the mid-latitude compared to SAGE II extinction even after 4 years, suggesting that the sharp decay in S-burden observed by Baran and Foot (1994) may be unrealistic. Interestingly, in the SH mid latitudes, extinction from **Pin14** shows much better agreement with SAGE II extinctions at 20 and 24 km. This again confirms biases discussed in Figure 2 that could be attributed to the weaker lower stratospheric transport in the SH mid-latitudes. At 1020 nm, agreement is even better (See Supplementary Figure S1). Also as observed in Figure 1 and 2, extinction differences between runs **Pin10**, **Pin14** and **Pin20** are largest for the first few months after the eruption but extinction lines almost overlap within ensemble variance from each eruption. This again confirms that the more SO_2 injection, the faster growth and removal within first few months after the eruption.

One of the key feature seen in Figure 3 that is not captured well in any model simulation is the plateau in the SAGE II (and GloSSAC) tropical peak extinction. For example, at 24 km (where the effect of instrument saturation should be minimal), after reaching peak values within first 3 months, extinction values remain almost flat for at least 6 months. At 20 km, this plateau in extinction in the tropics is visible for almost 12 months in the GloSSAC data (not shown). Similar features are visible at 1020 nm extinction (Figure S1). If indeed these plateau features are realistic in observational data, then they would be maintained by balance between tropical up-welling (upward branch of the Brewer-Dobson circulation as well as one from aerosol-induced heating) and sedimentation of particles that have grown via coagulation. On the other hand, model-simulated extinction shows more prominent seasonal cycle fluctuations during NH winter when the Brewer Dobson circulation (tropical upwelling) is strongest (e.g. Dhomse et al., 2008; Weber et al., 2011; Butchart, 2014). These plateau structures in extinctions are not so distinct at mid-latitudes in either hemisphere but seasonal cycle fluctuations that are determined by the wintertime circulation are visible in both SAGE II and model data. Another important difference is that modelled extinctions are low-biased (up to 50%) during pre-eruption months. This could be associated with low background S-burden in our model or slightly elevated stratospheric aerosol due to small volcanic eruptions (such as Kelud,1990) that are not present in our simulations. Another explanation could be due to the fact that model not resolving the uptake of organics, with observations Murphy et al. (2007) and modelling (Yu et al., 2016) suggesting organic-sulphate particles (Murphy et al., 2014) are the dominant aerosol type in the tropical and mid-latitude upper troposphere and lower stratosphere.

Next, we compare effective radius (Reff) at similar altitudes. Figure 4 shows zonal mean Reff at 20 and 25 km from runs **Pin10** and **Pin14**. along with observation-based Reff described in Luo (2016). As shown in previous sections, **Pin20** clearly shows a high bias compared to S-burden, $sAOD_{550}$ as well as extinction observations, hence it is excluded in Figure 4. Overall, the temporal and spatial evolution of Reff estimated using observational data seems to be well captured in **Pin14** compared to **Pin20** (although Reff magnitude is high-biased by about 10%). Another important feature is that Reff at 25 km in the model simulations persists much longer than CMIP6 Reff. It is important to note that Russell et al. (1996) analysed a range of in-situ and ground-based remote sensing measurements from the post-Pinatubo period, showing that optical depth spectra observed

https://doi.org/10.5194/acp-2020-344
Preprint. Discussion started: 6 May 2020


Atmospheric Chemistry and Physics Discussions

from Mauna Loa are consistent with Reff values of 0.6 to 0.8 microns continuing until mid to late 1992 at this near-tropical latitude, with dust-sonde (OPC) measurements from Laramie balloon soundings measurements also showing Reff of 0.4 to 0.6 microns in the mid-latitude lower stratosphere. Hence, Reff enhancement after Pinatubo, in CMIP and model simulation are broadly in good agreement with the measurements analysed in Russell et al. (1996). And this clearly shows significant improvement since Dhomse et al. (2014) where Reff was underestimated by about 50%. The updated comparison to the Bauman et al. (2003) Reff dataset, derived from SAGE II and CLAES measurements, is shown in Supplementary Figure S4 These improvements were noticed during model development after Dhomse et al. (2014) to include meteoric smoke particles and their interactions at version 8.2 of the GLOMAP codebase (Brooke et al., 2017; Mann et al., 2019a; Marshall et al., 2019).

In the tropics, where Reff increases are largest, the timeseries of Reff is noticeably different at 20km and 25km. At 25km, the model simulations are somewhat counter-intuitive. Initially, they show decrease in Reff, likely due to this central part of the volcanic cloud being younger (and smaller) particles formed as the oxidation of the volcanic SO_2 triggers extensive new particle formation. By contrast at 20km, below the altitude at which the volcanic plume detrains the SO_2 (injection height range is 21-23km) the effective radius shows a steady increase, as relatively larger particles sediment to these altitudes as the tropical volcanic aerosol reservoir progresses. There is a slow but substantial growth in the average particle size in this tropical Pinatubo cloud, with the 20km level reaching peak Reff values only during mid-1992, in contrast to the peak S-burden and $sAOD_{550}$ which have already peaked at this time, being in decay phase since the start of 1992.

Whereas the simulated peak Reff enhancement occurs by mid-1992 in the tropics, in the NH mid-latitudes, the peak Reff occurs at the time of the peak meridional transport, the Reff variation there mainly reflecting the seasonal cycle of the BD circulation (Butchart, 2014). The different timing of the volcanic Reff enhancement in the tropics and mid-latitudes is important when interpreting or interpolating the in-situ measurement record from the post-Pinatubo OPC soundings from Laramie. Russell et al. (1996) show the Reff values derived from the Mauna Loa ground-based remote sensing are substantially larger than those from the dust-sondes at Laramie. Model simulation confirms this inherent coupling between dynamics, circulation and microphysical growth processes causes a different relationship between the tropical to mid-latitude ratio in Reff in the upper and lower portions of the volcanic aerosol cloud.

An important aspect of volcanically enhanced stratospheric aerosol is that they provide surface area for catalytic ozone loss (e.g. Cadle et al., 1975; Hofmann and Solomon, 1989). Stratospheric sulphate area density comparison for three different months (December 91, June 1992 and December 1992) is shown in Figure 5. SAD derived using observational data (Arfeuille et al., 2014) also known as 3λ SAD is also shown. Again, **Pin20** SAD shows a high biases, whereas **Pin10** SAD seems to show good agreement with 3λ data. Our simulations do not include the SO_2 injection from the August 1991 Mt. Hudson eruption (Chile), and yet the model captures well the volcanic SAD enhancement in the SH mid-latitude stratosphere. The model does not capture the enhanced SAD signal at 10-12km in the Southern Hemisphere in December 1991, the altitude of that feature in the 3λ dataset consistent with lidar measurements of the Hudson cloud from Aspendale, Australia (Barton et al., 1992). The most critical differences are that 3λ SAD are confined in the lowermost stratosphere, deeper cloud of enhanced SAD, with steeper low-high latitude SAD gradients are visible in all the model simulations. As seen in Figure 3, by June 1992 tropical SAD from runs **Pin10** and **Pin14** are low-biased indicating lower aerosol in the tropical pipe which could be either due to faster

https://doi.org/10.5194/acp-2020-344
Preprint. Discussion started: 6 May 2020


Atmospheric Chemistry and Physics Discussions

transport to the high latitudes (weaker subtropical barrier in the middle stratosphere) and/or quicker coagulation thereby faster sedimentation.

Figure 6 shows the time series of observed SW and LW radiative near-global mean flux anomalies (60°S - 60°N), with respect to a 1985 to 1989 (pre-Pinatubo) baseline. ERBE (black symbols) data is from Edition 3 Revision 1, non-scanner, wide field of-view observations (Wielicki et al., 2002). Coloured lines indicate ensemble mean forcings anomalies from three Pinatubo SO_2 emission scenarios. The Pin10 simulation generates a peak solar dimming of 4 W/m2, matching well both the timing and magnitude of the peak in the ERBE SW anomaly timeseries. It is notable that if the ERBE SW anomaly is calculated relative the 1995-1997 baseline, we see a peak solar dimming of 5.5 W/m2 (not shown), which then compares best with the Pinatubo SW forcing from Pin14. Consistently with the the S-burden, sAOD550 and mid-visible extinction comparisons (Figures 1, 2 and 3), the Pin20 simulation also overpredicts the magnitude of the Pinatubo forcing compared to ERBE. It is important to note here that the model Pinatubo forcings are not only from the volcanic aerosol cloud, but include also any effects from the simulated post-Pinatubo changes in other climate forcers (e.g. stratospheric ozone and water vapour). As expected run **Pin20** shows largest anomalies in both SW and LW radiation and distinct differences between **Pin10**, **Pin14** and **Pin20** are visible until the end of 1992. For this 10 to 20Tg emission range, we find the global-mean SW forcing scales approximately linearly with increasing SO2 emission amount, the 40% increase from 10 to 14Tg and 43% increase from 14 to 20Tg causing the Pinatubo SW forcing to be stronger by 34% (4.1 to 5.5 W/m2) and 36% (5.5 to 7.5 W/m2) respectively.

In contrast to the SW forcings, the magnitude of the anomaly in the peak LW forcing is best matched in the Pin20 simulation, although the Pin14 simulation also agrees quite well with the ERBE anomaly timeseries. Whereas the Pinatubo SW forcing will follow closely the mid-visible aerosol changes, the LW forcing is more complex to interpret, simulated LW aerosol absorption not analysed in this paper, and almost certainly having a different temporal variation than the 550 nm and 1020 nm extinction variations analysed here. Also, the model LW forcing also includes effects from the dynamical changes in stratospheric water vapour which partially offsets the SW dimming (e.g. Joshi et al., 2003) adding to the LW aerosol effect. Our simulations do not include co-emission of water vapour, which might have influened stratospheric chemistry (e.g. LeGrande et al., 2016) and altered observed Pinatubo forcing. Another possible explanation for this discrepancy might be much weaker signal in LW radiation alongside ERBE temporal coverage (36 days vs 72 days). Again, as in the sulphur burden and extinction comparisons, after January 1992 observed SW anomalies seem to decay at a faster rate compared to all the model simulations.

Another important volcanic impact is the aerosol-induced heating in the lower stratosphere as large particles absorb outgoing LW radiation. Since the ERA-interim analysis assimilates radiosonde observations from large number of sites in the tropics, we can compare the temperature anomaly to the model predictions, as a further independent test. However, exact quantification of this mechanism is somewhat compilcated as the ERA-interim stratospheric temperature anomalies also includes influence from other chemical and dynamical changes such as variation in ozone and water vapour as well as QBO and ENSO related changes in tropical upwelling (e.g. Angell, 1997b; Randel et al., 2009). Assuming the 5-year anomalies will remove effects of some of the short-term processes. Modelled temperature anomalies are simply differences between the sensitivity (**Pin10**, **Pin14** and **Pin20**) and control (**Pin00**) simulations. Although we compare the simulated Pinatubo warming (temperature difference) to ERA-interim temperature anomalies, this is only intended to provide an approximate observational constraint for the magnitude

https://doi.org/10.5194/acp-2020-344
Preprint. Discussion started: 6 May 2020


Atmospheric Chemistry and Physics Discussions

of the effect and the altitude at which it reaches maximum. The **Pin10** simulation best captures the magnitude of the ERA-interim post-Pinatubo tropical temperature anomalies, and the model simulations and re-analysis both show maximum warming occurred in the 30 to 50 hPa range around 3-4 months after the eruption. The model predicts Pinatubo aerosol cloud continued to cause a substantial warming ($>$ 2 K) throughout 1992, that propagates downwards as in ERA-interim temperature anomalies.

4.2 El Chichón aerosol cloud

Whereas Pinatubo is often the main case study to evaluate interactive stratospheric aerosol models, El Chichón provides a different test for the models, its volcanic aerosol cloud dispersing almost exclusively to the NH. We also seek to understand whether the biases seen for Pinatubo (over-predicted tropical sAOD and discrepancy between literature estimates of SO2 emission and the peak global aerosol loading) are also seen for this alternative major eruption case.

Both El Chichón and Pinatubo eruptions occurred in the modern satellite era, however there are far fewer datasets available for the evaluation of El Chichón aerosol properties as it occurred in the important gap period between SAGE-I and SAGE II (see Thomason et al., 2018). Although there are quite extensive observational data records for the El Chichón volcanic aerosol clouds (e.g McCormick and Swissler, 1983; Hofmann and Rosen, 1983a), combining these data with satellite datasets would greatly reduce large uncertainties about the evolution of the El-Chichón aerosol cloud (e.g. Sato et al., 1993; SPARC, 2006).

Here, our analysis focuses primarily on comparing simulated mid-visible stratospheric AOD at 550 nm ($sAOD_{550}$) to the CMIP6 and Sato datasets. We also test the simulated vertical extent of the El Chichón cloud, comparing extinction at 20 km and 25 km to the SAGE II (and GloSSAC) data record, and compare the model's simulated warming in the tropical lower stratospheric to temperature anomalies in the ERA-Interim reanalyses.

Figure 8 compares ensemble mean $sAOD_{550}$ from **Elc05**, **Elc07**, **Elc10** and three observation-based datasets. Overall, there are significant differences between simulated $sAOD_{550}$ and the observations. The CMIP6 dataset enacts strongest solar dimming in NH mid-latitudes (peak $sAOD_{550}$ of 0.28), the tropical reservoir never exceeding a sAOD of 0.16, whereas the Sato and Ammann datasets, enact highest $sAOD_{550}$ in the tropics. The model simulations also find highest solar dimming occurred in the tropical reservoir, with the mean of the 5 Tg simulations predicting maximum $sAOD_{550}$ of about 0.28. With the QBO in westerly phase, and timing of eruption (4th April), BD circulation exported large fraction of the plume readily to the NH, but the meridional gradient in the solar dimming is an important uncertainty to address in future research

In the model, how deep the tropical volcanic aerosol reservoir that forms is closely linked to the altitude of the volcanic SO2 emission. We aligned our experiments with the ISA-MIP HErSEA experiment design (Timmreck et al., 2018), specifying a 24-27 km injection height based on the information from the airborne lidar measurements in the tropical stratosphere that provide the main constraint for the gap-filled dataset (see Figure 4.34 in the ASAP report (SPARC, 2006)). Balloon measurements from Southern Texas and Laramie (Hofmann and Rosen, 1983b), and the constraints from the airborne lidar survey flights in July, September and October (McCormick and Swissler, 1983) will likely provide a good constraint for the interactive models, showing that a large part of the plume was transported to NH mid-high latitudes via middle branch of the Brewer Dobson circulation at around 25km, the lower altitudes of the cloud remaining confined to the tropical reservoir. The evolution of the cloud is complex and strongly influenced by several effects: the rate of SO_2 conversion to aerosol and the depletion of

https://doi.org/10.5194/acp-2020-344
Preprint. Discussion started: 6 May 2020


Atmospheric Chemistry and Physics Discussions

oxidants, the tropical upwelling of the Brewer Dobson circulation, sedimentation of the ash and sulphuric acid droplets (and their interactions) and the downward propagating QBO. The multiple interacting processes within the tropical reservoir make analysing this early phase dispersion a complex problem, yet their combined net effects determines the subsequent transport of the aerosol to mid-latitudes, and the radiative forcing that results.

Due to significant differences observed in Figure 8, even with limited SAGE II observations, simulated extinctions are compared in Figure 9. Simulated extinctions for all three SO_2 emission scenarios show an excellent agreement with SAGE II from October 1984 onwards. A sudden jump in the GloSSAC data at the start of the SAGE II period is evident, and other unexplained sudden increases in extinction earlier in the CMIP6 dataset, e.g. in the SH at 24km. On the other hand, somewhat elevated SAGE II extinction in the NH mid-latitudes compared to model extinctions highlight possible model discrepancy due to injection altitude leading faster removal. GloSSAC extinction in the SH mid-latitude shows very little seasonal variation, and the sudden changes seen at both 20 and 24km are surprising and difficult to reconcile with expected variation, and could potentially be artefacts from the interpolation procedure. Overall, Figure 9 clearly suggests potential areas where combining with models may help improve the GloSSAC (and other) datasets, highlighting the need for combining observational data with El Chichón-related model simulations to better represent the consistency and variations within the El Chichón surface cooling included in climate models.

Figure 10 shows the tropical warming of the stratosphere predicted by the model, comparing again to the ERA-interim temperature anomaly (compared to the mean for 1982-1986). As in Pinatubo case (Figure 7), the speed of downward propagation of these anomalies seems to be well captured by all the simulations. Peak warming of about 3 K observed in ERA-interim between 30-50 hPa seems to be well reproduced in **Elc07**. Warm anomalies (up to 1 K) visible in ERA-interim data between 10-20 hPa suggest the downward propagating westerly QBO contributed to up to 1 K warming, hence simulated warming will be about 1K less than the ERA-interim anomalies. Overall, **Elc05** seems to reproduce El Chichón-related warming more realistically but the slight warming persisting near 70 hPa until March 1983 is absent in this simulation. Again this suggest that for UM-UKCA, 5 Tg and 7 Tg are reasonable lower and upper limits of SO_2 injection required to simulate observed lower stratospheric warming.

4.3 Mt. Agung aerosol cloud

The El Chichon and Pinatubo eruptions occurred when satellite instruments were monitoring the stratospheric aerosol layer, and the global dispersion of their volcanic aerosol clouds are relatively well characterised For the Agung period our knowledge of the global dispersion is less certain and primarily based on the synthesis of surface radiation measurements from Dyer and Hicks (1968). These measurements show the Agung cloud dispersed mainly to the SH, although aerosol measurements from 10 balloon-borne particle counter soundings from Minneapolis in 1963-65 (Rosen, 1964, 1968) and ground-based lidar from Lexington, Massachussetts in 1963 and 1964 (Grams and Fiocco, 1967) show substantial enhancement in the NH as well. For this period, the Sato forcing dataset enacts solar dimming following the ground-based solar radiation measurements discussed in Dyer and Hicks (1968), whereas the CMIP6 dataset is based on simulations with a 2D interactive stratospheric aerosol model.

https://doi.org/10.5194/acp-2020-344
Preprint. Discussion started: 6 May 2020


Atmospheric Chemistry and Physics Discussions

To address these limitations, SPARC (Stratosphere-Troposphere Process and their Role in Climate Project) project entitled SSiRC (Stratospheric Sulphur and its Role in Climate) initiated a stratospheric aerosol data rescue project (see http://www.sparc-ssirc.org/data/datarescueactivity.html). Its primary aim is to gather and in some cases re-calibrate post-Agung aerosol measurements from major volcanic periods to provide new constraints for stratospheric aerosol models. For example, ship-borne lidar measurements of the tropical volcanic aerosol reservoir after Pinatubo have recently been recovered (Antuna-Marrero et al., 2020; Mann et al., 2020). As part of this paper, we are contributing to this SSiRC activity and have recovered the Lexington post-Agung ground-based lidar measurement from Grams and Fiocco (1967) and use these to constrain the vertical extent of the Agung aerosol cloud.

Figure 11 compares $sAOD_{550}$ from model simulations with CMIP6, Sato and Ammann data. Both CMIP6 and Sato datasets suggest the tropical volcanic aerosol cloud dispersed rapidly, and almost exclusively, to the SH, consistent also with our understanding of QBO-dependent meridional transport (Thomas et al., 2009). This means that during the westerly QBO phase the volcanic plume is quickly transported towards the winter hemisphere whereas during the easterly phase the tropics-to-high-latitude transport is slower, hence some part of the plume is available for the wintertime transport into the opposite hemisphere. In contrast, the Ammann dataset suggests a significant part of the cloud was transported to the NH, the dispersion parameterisation considering only seasonal changes in stratospheric circulation. Hence, the modulation of meridional transport caused by the QBO, in the Agung case, increasing the export from low to mid-latitudes, is not represented in the Ammann dataset.

Figure 11 also shows that for the post-Agung period, there are very large differences in the $sAOD_{550}$ between CMIP6 and Sato data. Hence, climate simulations performed using these two forcing data sets would have significantly different response between two CMIP assessment. Overall, the CMIP6 dataset generates much stronger peak $sAOD_{550}$ than Sato, with a peak of around 0.4 in the tropics, a few months after the eruption. Sato data shows peak value of about 0.12, which suddenly drops to below 0.05 within couple of months. Then after there is a steady build-up with a local peak in $sAOD_{550}$ occurring in November 1963, 8 months after the eruption. The Sato dataset then enacts a much stronger second peak in tropical $sAOD_{550}$ in August-September 1964 that must be based on measurements from Kenya and the Congo (Dyer and Hicks, 1968). By contrast, CMIP6, based on the AER-2D model, predicts the Agung cloud dispersed rapidly to the SH with the tropical reservoir reducing to $sAOD_{550}$ of less than 0.05 at that time. Our simulations predict the Agung aerosol dispersed to the SH with similar timing to the CMIP6 dataset, but with a larger proportion remaining in the tropical reservoir. Similar to CMIP6 datasets our simulations also predict secondary $sAOD_{550}$ peak in SH mid-latitudes near 40°S. Although a similar pattern is produced in almost all simulations, $sAOD_{550}$ from **Agu12** seems to be in much better agreement with CMIP6 data.

These comparisons highlight that there is still substantial uncertainty about the global dispersion of the Agung cloud. However, there are extensive set of stratospheric aerosol measurements carried out during this period (see http://www.sparc-ssirc.org/data/datarescueactivity.html). Hence, there is potential to reduce this uncertainty combining these observations also with interactive stratospheric model simulations (Timmreck et al., 2018). Dyer and Hicks (1968) discuss the transport pathways for the volcanic aerosol, in relation to seasonal export from the tropical reservoir. Stothers (2001) analysed a range of measurements to derive the turbidity of the Agung cloud, but they neglected measurement from Kenya and Congo sites in their analysis,

https://doi.org/10.5194/acp-2020-344
Preprint. Discussion started: 6 May 2020


Atmospheric Chemistry and Physics Discussions

attributing a lower accuracy in those data. It is notable those observations were during the dry season, when other sources of aerosol could potentially have caused additional solar dimming. In terms of modeling, Niemeier et al. (2019) discussed possible implications of two separate Agung eruptions in 1963. They performed two model simulations, one with a single eruption and one with two separate eruptions on 17th March and 16th May with 4.7 Tg and 2.3 Tg SO_2 injection, respectively. They found significant differences between simulated aerosol properties and available evaluation datasets. They suggested that two separate eruptions are necessary to simulate the climatic impact. However, due to limited observational data they could not validate their model results extensively. They also discussed that simulated $sAOD_{550}$ differences with respect to evaluation data are larger than the differences between their two simulations. Pitari et al. (2016) also present global mean $sAOD_{550}$ changes after the Agung eruption with single eruption (12 Tg on 16 May 1963), but they did not show the latitudinal extent of the Agung volcanic cloud dispersion.

Figure 12 compares simulated and CMIP6 extinctions at 550 nm at 16, 20 and 24 km. As in previous figures tropical comparison is shifted upwards by 4 km. Overall, modelled and CMIP6 extinctions show almost identical decay rate. At 16 km, nearly all the model simulations show high bias compared to CMIP6 data and model extinction. On the other hand, at 20 km, tropical CMIP6 extinction seems to peak a bit later and there is better agreement in the mid-latitude extinction in both the hemispheres. The UM-UKCA extinctions reflect the primary influence from the QBO because of changing the sub-tropical edge of the tropical reservoir as well as peak wintertime meridional transport in either hemisphere. On the other hand, CMIP6 extinctions, show strong seasonal cycle in the tropics. The differences between our model and CMIP6 extinction must be primarily due to injection altitude and the simplified aerosol microphysical model used to construct CMIP6 data. Similar evolution is observed in the extinctions at 1020 nm as shown in supplementary Figure S3.

Figure 12 also shows the extinction from the early ground-based lidar at Lexington, Massachusetts (42°44' N, 71°15' W) as presented in Grams and Fiocco (1967). The method used to convert lidar backscatter to extinction is described in the Supplementary Material. Although lidar data shows large variability, these single location measurements still provide better insight about the transport of Agung aerosol cloud in the NH. At 16km, **Agu09** seem to show better agreement with lidar data, although by spring 1965, simulated extinctions are lower than the lidar data, suggesting faster decay in the model at this level. A similar pattern is observed at 20 km. The somewhat larger lidar extinction in spring 1965 compared to model simulations might be due to either weak model tropics-to-NH-mid-latitude transport (more transport to the SH), or aerosol removal is too fast in the simulations. Extinctions at 24 km are shown in supplementary Figure S4, and again confirm good agreement between lidar and **Agu09**. Overall, the extinction comparison with Lexington lidar data suggests that transport of the Agung volcanic cloud and its vertical extent in to the NH mid-latitude is well represented in **Agu09**.

Finally, we compare tropical warming in Figure 12. As ERA-Interim reanalyses start in 1979, hence we calculate observational-based anomalies from ERA–40 data. Bearing in mind that almost all the reanalysis datasets have significant inhomogeneities in the pre-satellite era, observation-based warming estimates should be treated carefully. However, as expected ERA-40 data show almost 1 K warming in the middle stratosphere before the eruption indicating downward propagation of warmer anomalies associated with the westerly QBO. Using radiosonde data, Free et al. (2009) estimated about 1.5 K warming near 50 hPa, which is somewhat consistent with ERA-40 (after removing 1 K warming due to westerly QBO). However, almost all

https://doi.org/10.5194/acp-2020-344
Preprint. Discussion started: 6 May 2020


Atmospheric Chemistry and Physics Discussions

of the simulations show 1-2 K more warming compared to ERA-40 data as modelled temperature differences do not include QBO-related anomalies.

5 Conclusions

We have applied the interactive stratospheric aerosol configuration of the UM-UKCA model to simulate the formation and global dispersion of the volcanic aerosol clouds from the three largest tropical eruptions of the 20th century, Agung, El Chichón and Pinatubo. The simulations are analysed to assess the evolution of each eruption cloud, from an initial tropical reservoir of volcanic aerosol to a hemispherically dispersed stratospheric aerosol cloud. For each eruption, 3-member ensembles are carried out for each of upper, lower and mid-point of the literature range of SO_2 emission, aligning with the design of the co-ordinated HErSEA experiment, part of the multi-model ISA-MIP interactive stratospheric aerosol modelling initiative (see Timmreck et al., 2018). The analysis is also designed to provide new "microphysically-consistent and observationally-constrained" volcanic forcing datasets for climate models, to represent each eruption's surface cooling more realistically.

Simulated aerosol optical properties are compared against a range of satellite datasets. The model captures the observed variation in global stratospheric sulphur from 1991-3 HIRS measurements very well, and experiments **Pin10** and **Pin14** defining a model-specific 10 to 14 Tg emissions uncertainty range and identifying a potential weighting to define a best-fit forcing dataset for Pinatubo. Our simulations also show that the aerosol decay rate is inversely proportional to the SO_2 injection amount, illustrating how increased aerosol particle size causes faster sedimentation. The model ensembles compares very well to mid-visible and near-infra-red aerosol extinction from SAGE II measurements. Although, the model shows higher sAOD biases in the tropics, it is common feature seen in interactive stratospheric aerosol models (e.g. Mills et al., 2016; Sukhodolov et al., 2018; Niemeier et al., 2019). We have also compared the Pinatubo ensembles to the three widely used forcing datasets (CMIP6–GloSSAC, Sato and Ammann) and we find that **Pin14** model ensemble shows overall best agreement. A plateau in lower stratospheric tropical extinction seen in GloSSAC data for almost one year after the Pinatubo eruption, is not reproduced in our simulations and thus remains as an open scientific question. The 10-14Tg SO_2 emissions rage for the model is lower than the 14-23 Tg observed to be present after the eruption (Guo et al., 2004b), and the tropical $sAOD_{550}$ high bias is consistent with the models missing an important removal process. Plausible suggestions for these are: a) the vertical redistribution of the volcanic cloud due to ash, b) changes in SO_2 oxidation due to OH decrease inside the plume, and c) too strong a subtropical barrier in the models.

The simulated Reff shows good agreement with CMIP6 data, the model simulates a deeper global layer of enhanced SAD than in the 3λ dataset (Luo, 2016). Simulated global-mean SW forcing (solar dimming) in run **Pin10** shows excellent agreement with the magnitude of the anomaly in the ERBE data, and the LW forcing in the model also matching well with the magnitude and shape of the ERBE anomaly. Assuming a 1 K colder temperature anomaly in ERA-Interim tropical temperatures due to the downward propagating QBO, a warming of 3 K near 50 hPa is well simulated in both **Pin10** and **Pin14** simulations. Overall, most of the comparisons suggest that about 10-14 Tg SO_2 injection between 21-23 km is sufficient to simulate the climate and chemical impact of the Mt. Pinatubo eruption.

https://doi.org/10.5194/acp-2020-344
Preprint. Discussion started: 6 May 2020


Atmospheric Chemistry and Physics Discussions

For the El Chichón eruption, there are significant differences between observation-based $sAOD_{550}$ estimates, hence evaluation of the simulations is somewhat restricted. However, NH mid-latitudes generally have a good quality observational data record, and $sAOD_{550}$ from run **Elc10** shows good agreement with CMIP6 data but run **Elc05** shows best agreement with Sato dataset in the tropics. Our extinction comparisons also show that there are inhomogeneities in the GloSSAC data during this period, hence El Chichón-related aerosol properties must be treated with caution. Based on comparisons of the lower stratospheric warming of about 2 K, 5 Tg and 7 Tg SO_2 injections seem to be reasonable lower and upper limits for what is required to simulate observed temperature changes.

Finally, evaluation of Mt. Agung aerosol is more complicated due to much larger differences in the observation-based datasets. Due to the westerly phase of QBO and timing of the eruption, CMIP6 data show a tropical peak in $sAOD_{550}$ within a month of the March eruption which is transported to SH mid-latitudes by October. Sato dataset suggest two peaks in the tropics 8 and 14 months after the eruption. Run **Agu06** shows reasonable agreement with limited amount of observational extinction data, although that is not conclusive. Comparison with the lidar measurements from Lexington suggests that the vertical extent of the Agung volcanic cloud in the NH mid-latitudes, is in good agreement with run **Agu09**. Comparisons with ERA-40 temperature anomalies also suggests that 3 K warming in the tropical stratosphere (2 K in the model simulation due to westerly phase of QBO). Assuming CMIP6-simulated $sAOD_{550}$ is realistic, 6 Tg and 9 Tg SO_2 injection seem to be the best lower and upper estimates required to simulate Mt. Agung-related aerosol in the UM-UKCA.

Overall, we have validated the interactive stratospheric aerosol configuration of the GA4 UM-UKCA model, and have shown the simulated aerosol properties for the Pinatubo ensemble are consistently in good agreement to a range of satellite-based observational datasets. For Pinatubo, we have also compared to three different independent tests of the radiative effects from the volcanic aerosol cloud: the ERBE flux anomaly timeseries in the SW and LW, and the stratospheric warming in the ERA-interim re-analysis. These comparisons confirm that a 10 to 14 Tg emission flux of SO_2 would accurately represent the effects the new forcing datasets would enact for Pinatubo in chemistry climate model integrations. For El Chichón and Agung, the magnitude of the volcanic forcing is highly uncertain, the volcanic aerosol datasets used in CMIP5 and CMIP6 historical integrations showing substantial differences. We contend there is substantial potential to improve on this situation, by identifying consensus forcings from multi-model simulations (Timmreck et al., 2018), with comparison to additional in-situ and active remote sensing measurements such as those being initiated within the SSiRC data rescue activity (Antuna-Marrero et al., 2020; Mann et al., 2020).

Data availability. Simulated aerosol data are publicly available from http://homepages.see.leeds.ac.uk/~fbsssdh/Dhomse2019_Volcanic_Aerosol_Data/ We will get doi for Data once manuscript is online

.

https://doi.org/10.5194/acp-2020-344
Preprint. Discussion started: 6 May 2020

Atmospheric Chemistry and Physics Discussions

Author contributions. SD and GM led the initial experiement design, model simulations, data analysis and the writing of the paper. The figures were prepared by SD. GM, SS and JCA retrieved and processed Lexington LIDAR data. GM, LM, LA and CJ contributed towards this GA4-UM-UKCA interactive stratospheric chemistry-aerosol model capability. All co-authors contributed re: either advising/co-ordinating the UKCA developments, writing sections of the paper, performing evaluation and/or reviewing drafts of the paper.

Competing interests. The authors declare that they have no conflict of interest.

Acknowledgements. We thank Dr. Larry Thomason (NASA Langley) and Dr. Beiping Luo (ETH-Zurich) for useful discussions about use of GloSSAC and CMIP6 datasets. We also acknowledge the contributions of James Brooke (Univ. Leeds), Nicolas Bellouin (Univ. Reading), Anja Schmidt (Univ. Cambridge) and Mohit Dalvi (Joint Weather and Climate Research Programme, UK Met Office) in contributing to help develop this interactive stratospheric chemistry-aerosol configuration of GA4-UM-UKCA. SD was supported by the NERC SISLAC project (NE/R001782/1). SD, GM and KC received funding via the NERC highlight topic consortium project SMURPHS ("Securing Multidisciplinary UndeRstanding and Prediction of Hiatus and Surge periods", NERC grant NE/N006038/1. GM also received funding from the NCAS, via the ACSIS long-term science programme on the Atlantic climate system. GM was also part-funded from the Copernicus Atmospheric Monitoring Service (CAMS), one of six services that form Copernicus, the European Union's Earth Observation programme. Juan Carlos Antuna-Marrero acknowledges travel and subsistence funding from CAMS that enabled his 1-month visit in March 2019 to the School of Earth and Environment (SEE), University of Leeds, with CAMS and SEE also co-funding Sarah Shallcross's PhD studentship. We thank the European Centre for Medium-Range Weather Forecasts for providing their ERA-interim meteorological re-analyses, which were obtained via the UK Centre for Environmental Data Access (CEDA). Simulations were performed on the UK ARCHER national supercomputing service and data analysis used the UK collaborative JASMIN data facility.

https://doi.org/10.5194/acp-2020-344
Preprint. Discussion started: 6 May 2020

Atmospheric Chemistry and Physics Discussions

References

Abraham, N. L., Archibald, A. T., Bellouin, N., Boucher, O., Braesicke, P., Bushell, A., Carslaw, K., Collins, B., Dalvi, M., Emmerson, K., and Others: Unified Model Documentation Paper No. 84: United Kingdom Chemistry and Aerosol (UKCA) Technical Description MetUM Version 8.4, UK Met Office, Exeter, UK, https://www.ukca.ac.uk/images/b/b1/Umdp{_}084-umdp84.pdf, 2012.

Ammann, C. M., Meehl, G. A., Washington, W. M., and Zender, C. S.: A monthly and latitudinally varying volcanic forcing dataset in simulations of 20th century climate, Geophysical Research Letters, 30, https://doi.org/10.1029/2003GL016875, http://doi.wiley.com/10.1029/2003GL016875, 2003.

Angell, J. K.: Stratospheric warming due to Agung, El Chichón, and Pinatubo taking into account the quasi-biennial oscillation, Journal of Geophysical Research: Atmospheres (1984–2012), 102, 9479–9485, https://doi.org/10.1029/96JD03588, http://onlinelibrary.wiley.com/doi/10.1029/96JD03588/full, 1997a.

Angell, J. K.: Estimated impact of Agung, El Chichon and Pinatubo volcanic eruptions on global and regional total ozone after adjustment for the QBO, Geophysical Research Letters, 24, 647–650, https://doi.org/10.1029/97GL00544, http://doi.wiley.com/10.1029/97GL00544, 1997b.

Antuña, J. C.: Lidar measurements of stratospheric aerosols from Mount Pinatubo at Camaguey, Cuba, in: Atmospheric Environment, vol. 30, pp. 1857–1860, Elsevier Ltd, https://doi.org/10.1016/1352-2310(95)00386-X, 1996.

Antuña, J. C.: Spatial and temporal variability of the stratospheric aerosol cloud produced by the 1991 Mount Pinatubo eruption, Journal of Geophysical Research, 108, 4624, https://doi.org/10.1029/2003JD003722, http://doi.wiley.com/10.1029/2003JD003722, 2003.

Antuña, J. C., Robock, A., Stenchikov, G. L., Thomason, L. W., and Barnes, J. E.: Lidar validation of SAGE II aerosol measurements after the 1991 Mount Pinatubo eruption, Journal of Geophysical Research Atmospheres, 107, 4194, https://doi.org/10.1029/2001JD001441, http://doi.wiley.com/10.1029/2001JD001441, 2002.

Antuna-Marrero, J. C., Mann, G. W., Keckhut, P., Avdyushin, S., Nardi, B., and Thomason, L. W.: Early ship borne lidar measurements of the Pinatbo in the Antarctic, Earth System Science Data, NA, NA—-NA, https://doi.org/10.xxxx/essd-submitted, https://www.earth-syst-sci-data.net, 2020.

Aquila, V., Oman, L. D., Stolarski, R., Douglass, A. R., and Newman, P. A.: The Response of Ozone and Nitrogen Dioxide to the Eruption of Mt. Pinatubo at Southern and Northern Midlatitudes, Journal of the Atmospheric Sciences, 70, 894–900, https://doi.org/10.1175/JAS-D-12-0143.1, http://journals.ametsoc.org/doi/abs/10.1175/JAS-D-12-0143.1, 2013.

Arfeuille, F., Luo, B. P., Heckendorn, P., Weisenstein, D., Sheng, J. X., Rozanov, E., Schraner, M., Brönnimann, S., Thomason, L. W., and Peter, T.: Modeling the stratospheric warming following the Mt. Pinatubo eruption: Uncertainties in aerosol extinctions, Atmospheric Chemistry and Physics, 13, 11 221–11 234, https://doi.org/10.5194/acp-13-11221-2013, https://www.atmos-chem-phys.net/13/11221/2013/http://www.atmos-chem-phys.net/13/11221/2013/acp-13-11221-2013.html, 2013.

Arfeuille, F. X., Weisenstein, D., MacK, H., Rozanov, E., Peter, T., and Brönnimann, S.: Volcanic forcing for climate modeling: a new microphysics-based data set covering years 1600–present, Climate of the Past, 10, 359–375, https://doi.org/10.5194/cp-10-359-2014, 2014.

Baran, A. J. and Foot, J. S.: New application of the operational sounder HIRS in determining a climatology of sulphuric acid aerosol from the Pinatubo eruption, Journal of Geophysical Research, 99, 25 673–25 679, https://doi.org/10.1029/94JD02044, http://doi.wiley.com/10.1029/94JD02044, 1994.

https://doi.org/10.5194/acp-2020-344
Preprint. Discussion started: 6 May 2020

Barnes, J. E. and Hofmann, D. J.: Lidar measurements of stratospheric aerosol over Mauna Loa Observatory, Geophysical Research Letters, 24, 1923–1926, https://doi.org/10.1029/97GL01943, 1997.

Barton, I. J., Prata, A. J., Watterson, I. G., and Young, S. A.: Identification of the Mount Hudson volcanic cloud over SE Australia, Geophysical Research Letters, 19, 1211–1214, https://doi.org/10.1029/92GL01122, http://doi.wiley.com/10.1029/92GL01122, 1992.

Bauman, J. J., Russell, P. B., Geller, M. A., and Hamill, P.: A stratospheric aerosol climatology from SAGE II and CLAES measurements: 1. Methodology, Journal of Geophysical Research: Atmospheres, 108, n/a–n/a, https://doi.org/10.1029/2002JD002992, http://doi.wiley.com/10.1029/2002JD002992, 2003.

Bekki, S., Toumi, R., and Pyle, J. A.: Role of Sulphur Photochemistry in Tropical Ozone Changes After the Eruption of Mount Pinatubo, Nature, 362, 331–333, https://doi.org/10.1038/362331a0, http://www.nature.com/doifinder/10.1038/362331a0, 1993.

Bittner, M., Schmidt, H., Timmreck, C., and Sienz, F.: Using a large ensemble of simulations to assess the Northern Hemisphere stratospheric dynamical response to tropical volcanic eruptions and its uncertainty, Geophysical Research Letters, 43, 9324–9332, https://doi.org/10.1002/2016GL070587, http://doi.wiley.com/10.1002/2016GL070587, 2016.

Brooke, J. S. A., Feng, W., Carrillo-Sánchez, J. D., Mann, G. W., James, A. D., Bardeen, C. G., Marshall, L., Dhomse, S. S., and Plane, J. M. C.: Meteoric Smoke Deposition in the Polar Regions: A Comparison of Measurements With Global Atmospheric Models, Journal of Geophysical Research: Atmospheres, 122, 11,111–112,130, https://doi.org/10.1002/2017JD027143, http://doi.wiley.com/10.1002/2017JD027143, 2017.

Butchart, N.: The Brewer-Dobson circulation, Reviews of Geophysics, 52, 157–184, https://doi.org/10.1002/2013RG000448, http://doi.wiley.com/10.1002/2013RG000448, 2014.

Cadle, R. D. and Grams, G. W.: Stratospheric aerosol particles and their optical properties, https://doi.org/10.1029/RG013i004p00475, 1975.

Cadle, R. D., Crutzen, P., and Ehhalt, D.: Heterogeneous chemical reactions in the stratosphere, Journal of Geophysical Research, 80, 3381–3385, https://doi.org/10.1029/jc080i024p03381, 1975.

Canty, T., Mascioli, N. R., Smarte, M. D., and Salawitch, R. J.: An empirical model of global climate – Part 1: A critical evaluation of volcanic cooling, Atmospheric Chemistry and Physics, 13, 3997–4031, https://doi.org/10.5194/acp-13-3997-2013, https://www.atmos-chem-phys.net/13/3997/2013/, 2013.

DallaSanta, K., Gerber, E. P., and Toohey, M.: The Circulation Response to Volcanic Eruptions: The Key Roles of Stratospheric Warming and Eddy Interactions, Journal of Climate, 32, 1101–1120, https://doi.org/10.1175/JCLI-D-18-0099.1, http://journals.ametsoc.org/doi/10.1175/JCLI-D-18-0099.1, 2019.

Damadeo, R. P., Zawodny, J. M., Thomason, L. W. L., and Iyer, N.: SAGE version 7.0 algorithm: application to SAGE II, Atmospheric Measurement Techniques, 6, 3539–3561, https://doi.org/10.5194/amt-6-3539-2013, http://www.atmos-meas-tech.net/6/3539/2013/amt-6-3539-2013.html, 2013.

Dee, D. P., Uppala, S. M., Simmons, A. J., Berrisford, P., Poli, P., Kobayashi, S., Andrae, U., Balmaseda, M. A., Balsamo, G., Bauer, P., Bechtold, P., Beljaars, A. C. M., van de Berg, L., Bidlot, J., Bormann, N., Delsol, C., Dragani, R., Fuentes, M., Geer, A. J., Haimberger, L., Healy, S. B., Hersbach, H., Hólm, E. V., Isaksen, L., Kållberg, P., Köhler, M., Matricardi, M., McNally, A. P., Monge-Sanz, B. M., Morcrette, J.-J. J., Park, B.-K. K., Peubey, C., de Rosnay, P., Tavolato, C., Thépaut, J.-N. N., and Vitart, F.: The ERA-Interim reanalysis: configuration and performance of the data assimilation system, Quarterly Journal of the Royal Meteorological Society, 137, 553–597, https://doi.org/10.1002/qj.828, http://doi.wiley.com/10.1002/qj.828, 2011.

https://doi.org/10.5194/acp-2020-344
Preprint. Discussion started: 6 May 2020

Dhomse, S., Weber, M., and Burrows, J.: The relationship between tropospheric wave forcing and tropical lower stratospheric water vapor, Atmospheric Chemistry and Physics, 8, 471–480, https://doi.org/10.5194/acp-8-471-2008, http://www.atmos-chem-phys.net/8/471/2008/acp-8-471-2008.html, 2008.

Dhomse, S., Chipperfield, M. P. M. P., Feng, W., and Haigh, J. D.: Solar response in tropical stratospheric ozone: a 3-D chemical transport model study using ERA reanalyses, Atmospheric Chemistry and Physics, 11, 12 773–12 786, https://doi.org/10.5194/acp-11-12773-2011, http://www.atmos-chem-phys.net/11/12773/2011/acp-11-12773-2011.html, 2011.

Dhomse, S., Chipperfield, M., Feng, W., Hossaini, R., Mann, G., and Santee, M.: Revisiting the hemispheric asymmetry in midlatitude ozone changes following the Mount Pinatubo eruption: A 3-D model study, Geophysical Research Letters, 42, 3038–3047, https://doi.org/10.1002/2015GL063052, http://doi.wiley.com/10.1002/2015GL063052, 2015.

Dhomse, S. S., Chipperfield, M. P., Feng, W., Ball, W. T., Unruh, Y. C., Haigh, J. D., Krivova, N. A., Solanki, S. K., and Smith, A. K.: Stratospheric O3 changes during 2001—2010: the small role of solar flux variations in a chemical transport model, Atmospheric Chemistry and Physics, 13, 10 113–10 123, https://doi.org/10.5194/acp-13-10113-2013, http://www.atmos-chem-phys.net/13/10113/2013/acp-13-10113-2013.html, 2013.

Dhomse, S. S., Emmerson, K. M., Mann, G. W., Bellouin, N., Carslaw, K. S., Chipperfield, M. P., Hommel, R., Abraham, N. L., Telford, P., Braesicke, P., Dalvi, M., Johnson, C. E., O'Connor, F., Morgenstern, O., Pyle, J. A., Deshler, T., Zawodny, J. M., and Thomason, L. W.: Aerosol microphysics simulations of the Mt.˜Pinatubo eruption with the UM-UKCA composition-climate model, Atmospheric Chemistry and Physics, 14, 11 221–11 246, https://doi.org/10.5194/acp-14-11221-2014, http://www.atmos-chem-phys.net/14/11221/2014/acp-14-11221-2014.html, 2014.

Driscoll, S., Bozzo, A., Gray, L. J., Robock, A., and Stenchikov, G.: Coupled Model Intercomparison Project 5 (CMIP5) simulations of climate following volcanic eruptions, Journal of Geophysical Research: Atmospheres, 117, D17 105, https://doi.org/10.1029/2012JD017607, http://doi.wiley.com/10.1029/2012JD017607, 2012.

Dyer, A.: ANISOTROPIC DIFFUSION COEFFICIENTS AND THE GLOBAL SPREAD OF VOLCANIC DUST, J Geophys Res, 75, 3007–3012, https://doi.org/10.1029/jc075i015p03007, 1970.

Dyer, A. J.: The effect of volcanic eruptions on global turbidity, and an attempt to detect long-term trends due to man, Quarterly Journal of the Royal Meteorological Society, 100, 563–571, https://doi.org/10.1002/qj.49710042606, http://doi.wiley.com/10.1002/qj.49710042606, 1974.

Dyer, A. J. and Hicks, B. B.: Global spread of volcanic dust from the Bali eruption of 1963, Quarterly Journal of the Royal Meteorological Society, 94, 545–554, https://doi.org/10.1002/qj.49709440209, http://doi.wiley.com/10.1002/qj.49709440209, 1968.

Eyring, V., Harris, N. R., Rex, M., Shepherd, T. G., Fahey, D. W., Amanatidis, G. T., Austin, J., Chipperfield, M. P., Dameris, M., Forster, P. M. F., Gettelman, A., Graf, H. F., Nagashima, T., Newman, P. A., Pawson, S., Prather, M. J., Pyle, J. A., Salawitch, R. J., Santer, B. D., and Waugh, D. W.: A strategy for process-oriented validation of coupled chemistry-climate models, Bulletin of the American Meteorological Society, 86, 1117–1133, https://doi.org/10.1175/BAMS-86-8-1117, 2005.

Eyring, V., Chipperfield, M. P., Giorgetta, M. A., Kinnison, D. E., Manzini, E., Newman, P. A., Shepherd, T. G., Waugh, D. W., Matthes, K., Newman, P. A., Pawson, S., Shepherd, T. G., and Waugh, D. W.: New CCMVal Reference and Sensitivity Simulations Overview of the New CCMVal Reference and Sensitivity Simulations in Support of Upcoming Ozone and Climate Assessments and the Planned SPARC CCMVal Report, SPARC Newsl, 30, 20–26, 2008.

Eyring, V., Lamarque, J.-F., Hess, P., Arfeuille, F., Bowman, K., Chipperfield, M. P., Duncan, B., Fiore, A., Gettelman, A., Giorgetta, M. A., Granier, C., Hegglin, M., Kinnison, D., Kunze, M., Langematz, U., Luo, B., Martin, R., Matthes, K., Newman, P. A., Peter,

https://doi.org/10.5194/acp-2020-344
Preprint. Discussion started: 6 May 2020

T., Peter, T., Robock, A., Ryerson, T., Saiz-Lopez, A., Salawitch, R., Schultz, M., Shepherd, T. G., Shindell, D., Staehelin, J., Tegtmeier, S., Thomason, L., Tilmes, S., Vernier, J.-P., Waugh, D., and Young, P.: Overview of IGAC/SPARC Chemistry-Climate Model Initiative (CCMI) Community Simulations in Support of Upcoming Ozone and Climate Assessments, http://oceanrep.geomar.de/20227/1/40{_}SPARCnewsletter{_}Jan2013{_}web.pdf, 2013.

Folland, C. K., Boucher, O., Colman, A., and Parker, D. E.: Causes of irregularities in trends of global mean surface temperature since the late 19th century, Science advances, 4, eaao5297, 2018.

Free, M., Lanzante, J., Free, M., and Lanzante, J.: Effect of Volcanic Eruptions on the Vertical Temperature Profile in Radiosonde Data and Climate Models, Journal of Climate, 22, 2925–2939, https://doi.org/10.1175/2008JCLI2562.1, http://journals.ametsoc.org/doi/abs/10.1175/2008JCLI2562.1, 2009.

Grainger, R. G., Lambert, A., Taylor, F. W., Remedios, J. J., Rodgers, C. D., Corney, M., and Kerridge, B. J.: Infrared absorption by volcanic stratospheric aerosols observed by ISAMS, Geophysical Research Letters, 20, 1283–1286, https://doi.org/10.1029/93GL00823, http://doi.wiley.com/10.1029/93GL00823, 1993.

Grams, G. and Fiocco, G.: Stratospheric aerosol layer during 1964 and 1965, Journal of Geophysical Research, 72, 3523–3542, https://doi.org/10.1029/jz072i014p03523, http://onlinelibrary.wiley.com/doi/10.1029/JZ072i014p03523/full, 1967.

Guo, S., Bluth, G. J. S., Rose, W. I., Watson, I. M., and Prata, A. J.: Re-evaluation of SO2 release of the 15 June 1991 Pinatubo eruption using ultraviolet and infrared satellite sensors, Geochemistry, Geophysics, Geosystems, 5, n/a–n/a, https://doi.org/10.1029/2003GC000654, http://doi.wiley.com/10.1029/2003GC000654http://www.agu.org/pubs/crossref/2004/2003GC000654.shtml, 2004a.

Guo, S., Rose, W. I., Bluth, G. J. S., and Watson, I. M.: Particles in the great Pinatubo volcanic cloud of June 1991: The role of ice, Geochemistry Geophysics Geosystems, 5, 101 029/, https://doi.org/10.1029/2003GC000655, http://www.agu.org/pubs/crossref/2004/2003GC000655.shtml, 2004b.

Hofmann, D. J. and Rosen, J. M.: Sulfuric acid droplet formation and growth in the stratosphere after the 1982 eruption of El Chichon, Science, 222, 325–327, 1983a.

Hofmann, D. J. and Rosen, J. M. J.: Stratospheric sulfuric acid fraction and mass estimate for the 1982 volcanic eruption of El Chichon, Geophysical research letters, 10, 313–316, https://doi.org/10.1029/GL010i004p00313, http://doi.wiley.com/10.1029/GL010i004p00313, 1983b.

Hofmann, D. J. and Solomon, S.: Ozone destruction through heterogeneous chemistry following the eruption of El Chichón, Journal of Geophysical Research, 94, 5029, https://doi.org/10.1029/JD094iD04p05029, http://doi.wiley.com/10.1029/JD094iD04p05029, 1989.

Holton, J. R., Haynes, P. H., McIntyre, M. E., Douglass, A. R., Rood, R. B., and Pfister, L.: Stratosphere-troposphere exchange, Reviews of Geophysics, 33, 403–439, https://doi.org/10.1029/95RG02097, http://www.agu.org/pubs/crossref/1995/95RG02097.shtml, 1995.

Hommel, R., Timmreck, C., and Graf, H. F.: The global middle-atmosphere aerosol model MAECHAM5-SAM2: comparison with satellite and in-situ observations, Geoscientific Model Development, 4, 809–834, https://doi.org/10.5194/gmd-4-809-2011, https://www.geosci-model-dev.net/4/809/2011/, 2011.

Jones, A. C., Haywood, J. M., Jones, A., and Aquila, V.: Sensitivity of volcanic aerosol dispersion to meteorological conditions: A Pinatubo case study, Journal of Geophysical Research: Atmospheres, 121, 6892–6908, https://doi.org/10.1002/2016JD025001, http://doi.wiley.com/10.1002/2016JD025001, 2016.

Joshi, M. M., Shine, K. P., Joshi, M. M., and Shine, K. P.: A GCM Study of Volcanic Eruptions as a Cause of Increased Stratospheric Water Vapor, http://dx.doi.org/10.1175/1520-0442(2003)016<3525:AGSOVE>2.0.CO;2, https://doi.org/10.1175/1520-0442(2003)016<3525:AGSOVE>2.0.CO;2, 2003.

https://doi.org/10.5194/acp-2020-344
Preprint. Discussion started: 6 May 2020

Kinne, S., Toon, O. B., and Prather, M. J.: Buffering of stratospheric circulation by changing amounts of tropical ozone - A Pinatubo case study, Geophysical Research Letters, 19, 1927–1930, https://doi.org/10.1029/92GL01937, http://doi.wiley.com/10.1029/92GL01937, 1992.

Kremser, S., Thomason, L. W., von Hobe, M., Hermann, M., Deshler, T., Timmreck, C., Toohey, M., Stenke, A., Schwarz, J. P., Weigel, R., Fueglistaler, S., Prata, F. J., Vernier, J. P., Schlager, H., Barnes, J. E., Antuña-Marrero, J. C., Fairlie, D., Palm, M., Mahieu, E., Notholt, J., Rex, M., Bingen, C., Vanhellemont, F., Bourassa, A., Plane, J. M., Klocke, D., Carn, S. A., Clarisse, L., Trickl, T., Neely, R., James, A. D., Rieger, L., Wilson, J. C., and Meland, B.: Stratospheric aerosol—Observations, processes, and impact on climate, https://doi.org/10.1002/2015RG000511, 2016.

Lacis, A., Hansen, J., and Sato, M.: Climate forcing by stratospheric aerosols, Geophysical Research Letters, 19, 1607–1610, https://doi.org/10.1029/92GL01620, http://doi.wiley.com/10.1029/92GL01620, 1992.

Lambert, A., Grainger, R. G., Remedios, J. J., Rodgers, C. D., Corney, M., and Taylor, F. W.: Measurements of the evolution of the Mt. Pinatubo aerosol cloud by ISAMS, Geophysical Research Letters, 20, 1287–1290, 1993.

Lambert, A., Grainger, R. G., Rodgers, C. D., Taylor, F. W., Mergenthaler, J. L., Kumer, J. B., and Massie, S. T.: Global evolution of the Mt Pinatubo volcanic aerosols observed by the infrared limb-sounding instruments CLAES and ISAMS on the Upper Atmosphere Research Satellite, Journal of Geophysical Research - Atmospheres, 102, 1495–1512, 1997.

Lee, H. and Smith, A.: Simulation of the combined effects of solar cycle, quasibiennial oscillation, and volcanic forcing on stratospheric ozone changes in recent decades, Journal of Geophysical Research, 108, 1–16, https://doi.org/10.1029/2001JD001503, http://onlinelibrary.wiley.com/doi/10.1029/2001JD001503/full, 2003.

LeGrande, A. N., Tsigaridis, K., and Bauer, S. E.: Role of atmospheric chemistry in the climate impacts of stratospheric volcanic injections, Nature Geoscience, https://doi.org/10.1038/ngeo2771, http://www.nature.com/doifinder/10.1038/ngeo2771, 2016.

Long, C. S. and Stowe, L. L.: Using the NOAA/AVHRR to study stratospheric aerosol optical thicknesses following the Mt Pinatubo eruption, Geophysical Research Letters, 21, 2215–2218, http://onlinelibrary.wiley.com/doi/10.1029/94GL01322/full, 1994.

Luo, B.: Stratospheric aerosol data for use in CMIP6 models, ftp://iacftp.ethz.ch/pub{_}read/luo/CMIP6/Readme{_}Data{_}Description.pdf, 2016.

Mann, G., Dhomse, S., Deshler, T., Timmreck, C., Schmidt, A., Neely, R., and Thomason, L.: Evolving particle size is the key to improved volcanic forcings, Past Global Change Magazine, 23, 52–53, https://doi.org/10.22498/pages.23.2.52, http://www.pastglobalchanges.org/products/pages-magazine/7166, 2015.

Mann, G., Brooke, J., Sengupta, K., Marshall, L., Dhomse, S., Feng, W., Neely, R., Bardeen, C., Bellouin, N., Dalvi, M., and Others: The prevalence of meteoric-sulphuric particles within the stratospheric aerosol layer and their influence on how pure sulphuric particles are transported and transformed., in: Geophysical Research Abstracts, vol. 21, 2019a.

Mann, G. W., Shallcross, S., Antuña-Marrero, J. C., Dhomse, S., Schmidt, A., Neely, R., Carslaw, K. S., Bellouin, N., Winker, D. M., Vaughan, G., and Others: Ash-sulphuric interactions: Simulating major volcanic aerosol clouds as global dust veils, in: AGU Fall Meeting 2019, 2019b.

Mann, G. W., Antuña-Marrero, J. C., Shallcross, S., Dhomse, S., Thomason, L., Beiping, L., Deshler, T., and Rosen, J.: Recovered measurements of the 1960s stratospheric aerosol layer for new constraints for volcanic forcing in the years after 1963 Agung, in: EGU Assembly 2020, 2020.

Marotzke, J. and Forster, P. M.: Forcing, feedback and internal variability in global temperature trends, Nature, 517, 565–570, https://doi.org/10.1038/nature14117, http://www.nature.com/articles/nature14117, 2015.

https://doi.org/10.5194/acp-2020-344
Preprint. Discussion started: 6 May 2020

Atmospheric Chemistry and Physics Discussions

Marshall, L., Schmidt, A., Toohey, M., Carslaw, K., Mann, G., Sigl, M., Khodri, M., Timmreck, C., Zanchettin, D., Ball, W., Bekki, S., Brooke, J., Dhomse, S., Johnson, C., Lamarque, J.-F., Legrande, A., Mills, M., Niemeier, U., Pope, J., Poulain, V., Robock, A., Rozanov, E., Stenke, A., Sukhodolov, T., Tilmes, S., Tsigaridis, K., and Tummon, F.: Multi-model comparison of the volcanic sulfate deposition from the 1815 eruption of Mt. Tambora, Atmospheric Chemistry and Physics, 18, https://doi.org/10.5194/acp-18-2307-2018, 2018.

Marshall, L., Johnson, J. S., Mann, G. W., Lee, L., Dhomse, S. S., Regayre, L., Yoshioka, M., Carslaw, K. S., and Schmidt, A.: Exploring How Eruption Source Parameters Affect Volcanic Radiative Forcing Using Statistical Emulation, Journal of Geophysical Research: Atmospheres, https://doi.org/10.1029/2018JD028675, http://doi.wiley.com/10.1029/2018JD028675, 2019.

McCormick, M.: Sage II: An overview, Advances in Space Research, 7, 219–226, https://doi.org/10.1016/0273-1177(87)90151-7, https://www.sciencedirect.com/science/article/pii/0273117787901517, 1987.

McCormick, M. P. and Swissler, T. J.: Stratospheric aerosol mass and latitudinal distribution of the El Chichon eruption cloud for October 1982, Geophysical research letters, 10, 877–880, 1983.

McCormick, M. P., Thomason, L. W., and Trepte, C. R.: Atmospheric effects of the Mt Pinatubo eruption, Nature, 373, 399–404, https://doi.org/10.1038/373399a0, http://jack.pixe.lth.se/kfgu/KOO090{_}FKF075/Artiklar/P05.pdfhttp://www.nature.com/articles/373399a0, 1995.

Mills, M. J., Schmidt, A., Easter, R., Solomon, S., Kinnison, D. E., Ghan, S. J., Neely, R. R., Marsh, D. R., Conley, A., Bardeen, C. G., and Gettelman, A.: Global volcanic aerosol properties derived from emissions, 1990-2014, using CESM1(WACCM), Journal of Geophysical Research: Atmospheres, 121, 2332–2348, https://doi.org/10.1002/2015JD024290, http://doi.wiley.com/10.1002/2015JD024290, 2016.

Morgenstern, O., Braesicke, P., O'Connor, F. M., Bushell, A. C., Johnson, C. E., Osprey, S. M., and Pyle, J. A.: Evaluation of the new UKCA climate-composition model – Part 1: The stratosphere, Geoscientific Model Development, 2, 43–57, https://doi.org/10.5194/gmd-2-43-2009, http://www.geosci-model-dev.net/2/43/2009/, 2009.

Morgenstern, O., Akiyoshi, H., Bekki, S., Braesicke, P., Butchart, N., Chipperfield, M. P., Cugnet, D., Deushi, M., Dhomse, S. S., Garcia, R. R., Gettelman, A., Gillett, N. P., Hardiman, S. C., Jumelet, J., Kinnison, D. E., Lamarque, J. F., Lott, F., Marchand, M., Michou, M., Nakamura, T., Olivié, D., Peter, T., Plummer, D., Pyle, J. A., Rozanov, E., Saint-Martin, D., Scinocca, J. F., Shibata, K., Sigmond, M., Smale, D., Teyssèdre, H., Tian, W., Voldoire, A., and Yamashita, Y.: Anthropogenic forcing of the Northern Annular Mode in CCMVal-2 models, Journal of Geophysical Research, 115, 1–15, https://doi.org/10.1029/2009JD013347, http://www.agu.org/pubs/crossref/2010/2009JD013347.shtml, 2010.

Morgenstern, O., Hegglin, M., Rozanov, E., O'Connor, F., Luke Abraham, N., Akiyoshi, H., Archibald, A., Bekki, S., Butchart, N., Chipperfield, M., Deushi, M., Dhomse, S., Garcia, R., Hardiman, S., Horowitz, L., Jöckel, P., Josse, B., Kinnison, D., Lin, M., Mancini, E., Manyin, M., Marchand, M., Marécal, V., Michou, M., Oman, L., Pitari, G., Plummer, D., Revell, L., Saint-Martin, D., Schofield, R., Stenke, A., Stone, K., Sudo, K., Tanaka, T., Tilmes, S., Yamashita, Y., Yoshida, K., and Zeng, G.: Review of the global models used within phase 1 of the Chemistry-Climate Model Initiative (CCMI), Geoscientific Model Development, 10, 639–671, https://doi.org/10.5194/gmd-10-639-2017, 2017.

Murphy, D. M., Cziczo, D. J., Hudson, P. K., and Thomson, D. S.: Carbonaceous material in aerosol particles in the lower stratosphere and tropopause region, Journal of Geophysical Research, 112, D04 203, https://doi.org/10.1029/2006JD007297, http://doi.wiley.com/10.1029/2006JD007297, 2007.

Murphy, D. M., Froyd, K. D., Schwarz, J. P., and Wilson, J. C.: Observations of the chemical composition of stratospheric aerosol particles, Quarterly Journal of the Royal Meteorological Society, 140, 1269–1278, https://doi.org/10.1002/qj.2213, http://doi.wiley.com/10.1002/qj.2213, 2014.

https://doi.org/10.5194/acp-2020-344
Preprint. Discussion started: 6 May 2020

Atmospheric Chemistry and Physics Discussions

Niemeier, U., Timmreck, C., and Krüger, K.: Revisiting the Agung 1963 volcanic forcing – impact of one or two eruptions, Atmospheric Chemistry and Physics, 19, 10 379–10 390, https://doi.org/10.5194/acp-19-10379-2019, https://www.atmos-chem-phys.net/19/10379/2019/, 2019.

O'Connor, F. M., Johnson, C. E., Morgenstern, O., Abraham, N. L., Braesicke, P., Dalvi, M., Folberth, G. A., Sanderson, M. G., Telford, P. J., Voulgarakis, A., Young, P. J., Zeng, G., Collins, W. J., and Pyle, J. A.: Evaluation of the new UKCA climate-composition model – Part 2: The Troposphere, Geoscientific Model Development, 7, 41–91, https://doi.org/10.5194/gmd-7-41-2014, https://www.geosci-model-dev.net/7/41/2014/, 2014.

Pitari, G., Cionni, I., Di Genova, G., Visioni, D., Gandolfi, I., and Mancini, E.: Impact of Stratospheric Volcanic Aerosols on Age-of-Air and Transport of Long-Lived Species, Atmosphere, 7, 149, https://doi.org/10.3390/atmos7110149, http://www.mdpi.com/2073-4433/7/11/149, 2016.

Pitts, M. C. and Thomason, L. W.: The impact of the eruptions of Mount Pinatubo and Cerro Hudson on antarctic aerosol levels during the 1991 austral spring, Geophysical Research Letters, 20, 2451–2454, 1993.

Plumb, R. A.: A "tropical pipe" model of stratospheric transport, Journal of Geophysical Research: Atmospheres, 101, 3957–3972, https://doi.org/10.1029/95JD03002, http://doi.wiley.com/10.1029/95JD03002, 1996.

Poberaj, C. S., Staehelin, J., and Brunner, D.: Missing Stratospheric Ozone Decrease at Southern Hemisphere Middle Latitudes after Mt. Pinatubo: A Dynamical Perspective, Journal of the Atmospheric Sciences, 68, 1922–1945, https://doi.org/10.1175/JAS-D-10-05004.1, http://journals.ametsoc.org/doi/abs/10.1175/JAS-D-10-05004.1, 2011.

Prather, M.: Catastrophic loss of stratospheric ozone in dense volcanic clouds, Journal of Geophysical Research, 97, 10 187–10 191, https://doi.org/10.1029/92jd00845, 1992.

Randel, W. J., Garcia, R. R., Calvo, N., and Marsh, D.: ENSO influence on zonal mean temperature and ozone in the tropical lower stratosphere, Geophysical Research Letters, 36, 1–5, https://doi.org/10.1029/2009GL039343, http://www.agu.org/pubs/crossref/2009/2009GL039343.shtml, 2009.

Robock, A.: Volcanic eruptions and climate, Reviews of Geophysics, 38, 191–219, https://doi.org/10.1029/1998RG000054, http://doi.wiley.com/10.1029/1998RG000054, 2000.

Robock, A. and Matson, M.: Circumglobal transport of the El Chichón volcanic dust cloud, Science, 221, 195–197, https://doi.org/10.1126/science.221.4606.195, 1983.

Roche, A. E., Kumer, J. B., Mergenthaler, J. L., Ely, G. A., Uplinger, W. G., Potter, J. F., James, T. C., and Sterritt, L. W.: The cryogenic limb array etalon spectrometer (CLAES) on UARS: Experiment description and performance, Journal of Geophysical Research, 98, 10 763, https://doi.org/10.1029/93JD00800, http://doi.wiley.com/10.1029/93JD00800, 1993.

Rosen, J.: The vertical distribution of dust to 30 kilometers, Journal of Geophysical Research, http://onlinelibrary.wiley.com/doi/10.1029/JZ069i021p04673/full, 1964.

Rosen, J.: Simultaneous dust and ozone soundings over North and Central America, Journal of Geophysical Research, 73, 479–486, 1968.

Rosen, J. M., Kjome, N. T., McKenzie, R. L., and Liley, J. B.: Decay of Mount Pinatubo Aerosol At Midlatitudes in the Northern and Southern Hemispheres, Journal Of Geophysical ResearchAtmospheres, 99, 25 733–25 739, http://onlinelibrary.wiley.com/doi/10.1029/94JD02312/full, 1994.

Russell, P. B., Livingston, J. M., Pueschel, R. F., Bauman, J. J., Pollack, J. B., Brooks, S. L., Hamill, P., Thomason, L. W., Stowe, L. L., Deshler, T., Dutton, E. G., and Bergstrom, R. W.: Global to microscale evolution of the Pinatubo volcanic aerosol derived from diverse

https://doi.org/10.5194/acp-2020-344
Preprint. Discussion started: 6 May 2020

measurements and analyses, Journal of Geophysical Research, 101, 18 745–18 763, https://doi.org/10.1029/96JD01162, http://doi.wiley.com/10.1029/96JD01162http://www.agu.org/pubs/crossref/1996/96JD01162.shtml, 1996.

Santer, B. D., Wigley, T. M. L., Doutriaux, C., Boyle, J. S., Hansen, J. E., Jones, P. D., Meehl, G. A., Roeckner, E., Sengupta, S., and Taylor, K. E.: Accounting for the effects of volcanoes and ENSO in comparisons of modeled and observed temperature trends, Journal of Geophysical Research: Atmospheres, 106, 28 033–28 059, https://doi.org/10.1029/2000JD000189, http://doi.wiley.com/10.1029/2000JD000189, 2001.

Santer, B. D., Bonfils, C., Painter, J. F., Zelinka, M. D., Mears, C., Solomon, S., Schmidt, G. A., Fyfe, J. C., Cole, J. N., Nazarenko, L., Taylor, K. E., and Wentz, F. J.: Volcanic contribution to decadal changes in tropospheric temperature, Nature Geoscience, 7, 185–189, https://doi.org/10.1038/ngeo2098, 2014.

Sato, M., Hansen, J. E. J. J. E., McCormick, M. P., and Pollack, J. B.: Stratospheric aerosol optical depths, 1850–1990, Journal of Geophysical Research, 98, 22 987, https://doi.org/10.1029/93JD02553, http://doi.wiley.com/10.1029/93JD02553, 1993.

Schmidt, G. A., Ruedy, R., Hansen, J. E., Aleinov, I., Bell, N., Bauer, M., Bauer, S., Cairns, B., Canuto, V., Cheng, Y., Del Genio, A., Faluvegi, G., Friend, A. D., Hall, T. M., Hu, Y., Kelley, M., Kiang, N. Y., Koch, D., Lacis, A. A., Lerner, J., Lo, K. K., Miller, R. L., Nazarenko, L., Oinas, V., Perlwitz, J., Perlwitz, J., Rind, D., Romanou, A., Russell, G. L., Sato, M., Shindell, D. T., Stone, P. H., Sun, S., Tausnev, N., Thresher, D., and Yao, M.-S.: Present-Day Atmospheric Simulations Using GISS ModelE: Comparison to In Situ, Satellite, and Reanalysis Data, Journal of Climate, 19, 153–192, https://doi.org/10.1175/JCLI3612.1, https://doi.org/10.1175/JCLI3612.1, 2006.

Sheng, J.-X., Weisenstein, D. K., Luo, B.-P., Rozanov, E., Arfeuille, F., and Peter, T.: A perturbed parameter model ensemble to investigate Mt. Pinatubo's 1991 initial sulfur mass emission, Atmospheric Chemistry and Physics, 15, 11 501–11 512, https://doi.org/10.5194/acp-15-11501-2015, https://www.atmos-chem-phys.net/15/11501/2015/, 2015a.

Sheng, J.-X. X., Weisenstein, D. K., Luo, B.-P. P., Rozanov, E., Stenke, A., Anet, J., Bingemer, H., and Peter, T.: Global atmospheric sulfur budget under volcanically quiescent conditions: Aerosol-chemistry-climate model predictions and validation, Journal of Geophysical Research: Atmospheres, 120, 256–276, https://doi.org/10.1002/2014JD021985, http://doi.wiley.com/10.1002/2014JD021985, 2015b.

Soden, B. J., Wetherald, R. T., Stenchikov, G. L., and Robock, A.: Global cooling after the eruption of Mount Pinatubo: a test of climate feedback by water vapor., Science, 296, 727–730, https://doi.org/10.1126/science.296.5568.727, http://www.ncbi.nlm.nih.gov/pubmed/11976452http://www.sciencemag.org/cgi/doi/10.1126/science.296.5568.727, 2002.

Solomon, S.: Stratospheric ozone depletion: A review of concepts and history, Reviews of Geophysics, 37, 275–316, https://doi.org/10.1029/1999RG900008, http://onlinelibrary.wiley.com/doi/10.1029/1999RG900008/full, 1999.

SPARC: SPARC Assessment of stratospheric aerosol properties (ASAP), Tech. rep., World Climate Research Programme, http://www.sparc-climate.org/publications/sparc-reports/sparc-report-no4/, 2006.

SPARC: SPARC Report on the Evaluation of Chemistry-Climate Models, in: SPARC report, vol. No. 5, p. 426 pp., World Climate Research Programme, wcrp - 30 edn., http://www.sparc-climate.org/publications/sparc-reports/sparc-report-no5/http://www.sparc-climate.org/publications/sparc-reports/, 2010.

Stenchikov, G. L. G. G. L., Kirchner, I., Robock, A., Graf, H.-F., Antuña, J. C., Grainger, R. G., Lambert, A., and Thomason, L.: Radiative forcing from the 1991 Mount Pinatubo volcanic eruption, Journal of Geophysical Research, 103, 13 837–13 857, https://doi.org/10.1029/98JD00693, http://www.agu.org/pubs/crossref/1998/98JD00693.shtmlhttp://onlinelibrary.wiley.com/doi/10.1029/98JD00693/full, 1998.

Stothers, R.: Major optical depth perturbations to the stratosphere from volcanic eruptions: Pyrheliometric period, 1881–1960, Journal of Geophysical Research: Atmospheres, http://onlinelibrary.wiley.com/doi/10.1029/95JD03237/full, 1996.

https://doi.org/10.5194/acp-2020-344
Preprint. Discussion started: 6 May 2020

Stothers, R. B.: Major optical depth perturbations to the stratosphere from volcanic eruptions: Stellar extinction period, 1961–1978, Journal of Geophysical Research: Atmospheres, 106, 2993–3003, https://doi.org/10.1029/2000JD900652, http://doi.wiley.com/10.1029/2000JD900652, 2001.

Sukhodolov, T., Sheng, J.-X., Feinberg, A., Luo, B.-P., Thomas, P., Revell, L., Stenke, A., Weisenstein, D. K., and Rozanov, E.: Stratospheric aerosol evolution after Pinatubo simulated with a coupled size-resolved aerosol-chemistry-climate model, SOCOL-AERv1. 0, Geoscientific Model Development, 11, 2633–2647, 2018.

Thomas, M. A., Giorgetta, M. A., Timmreck, C., Graf, H. F., and Stenchikov, G.: Simulation of the climate impact of Mt. Pinatubo eruption using ECHAM5 – Part 2: Sensitivity to the phase of the QBO and ENSO, Atmospheric Chemistry and Physics, 9, 3001–3009, https://doi.org/10.5194/acp-9-3001-2009, http://www.atmos-chem-phys.net/9/3001/2009/, 2009.

Thomason, L. W., Poole, L. R., and Deshler, T.: A global climatology of stratospheric aerosol surface area density deduced from stratospheric aerosol and gas experiment II measurements: 1984-1994, Journal of Geophysical ResearchAtmospheres, 102, 8967–8976, https://doi.org/10.1029/96JD02962, http://doi.wiley.com/10.1029/96JD02962, 1997.

Thomason, L. W., Ernest, N., Millán, L., Rieger, L., Bourassa, A., Vernier, J.-P., Manney, G., Luo, B., Arfeuille, F., and Peter, T.: A global space-based stratospheric aerosol climatology: 1979-2016, Earth System Science Data, 10, 469–492, 2018.

Timmreck, C., Mann, G. W., Aquila, V., Hommel, R., Lee, L. A., Schmidt, A., Brühl, C., Carn, S., Chin, M., Dhomse, S. S., Diehl, T., English, J. M., Mills, M. J., Neely, R., Sheng, J., Toohey, M., and Weisenstein, D.: The Interactive Stratospheric Aerosol Model Intercomparison Project (ISA-MIP): Motivation and experimental design, Geoscientific Model Development, 11, 2581–2608, https://doi.org/10.5194/gmd-11-2581-2018, 2018.

Trepte, C. C. R., Veiga, R. E., and McCormick, M. P.: The Poleward Dispersal of Mount Pinatubo Volcanic Aerosol, Journal of Geophysical Research, 98, 18 563–18 573, https://doi.org/10.1029/93JD01362, http://www.agu.org/pubs/crossref/1993/93JD01362.shtmlhttp://onlinelibrary.wiley.com/doi/10.1029/93JD01362/full, 1993.

Turco, R., Whitten, R., and Toon, O.: Stratospheric aerosols: Observation and theory, Reviews of Geophysics, http://onlinelibrary.wiley.com/doi/10.1029/RG020i002p00233/full, 1982.

Vaughan, G., Wareing, D. P., Jones, S. B., Thomas, L., and Larsen, N.: Lidar measurements of Mt. Pinatubo aerosols at Aberystwyth from August 1991 through March 1992, Geophysical Research Letters, 21, 1315–1318, https://doi.org/10.1029/93GL02893, http://doi.wiley.com/10.1029/93GL02893, 1994.

Walters, D. N., Williams, K. D., Boutle, I. A., Bushell, A. C., Edwards, J. M., Field, P. R., Lock, A. P., Morcrette, C. J., Stratton, R. A., Wilkinson, J. M., and Others: The Met Office Unified Model global atmosphere 4.0 and JULES global land 4.0 configurations, Geoscientific Model Development, 7, 361–386, 2014.

Weber, M., Dikty, S., Burrows, J. P., Garny, H., Dameris, M., Kubin, A., Abalichin, J., and Langematz, U.: The Brewer-Dobson circulation and total ozone from seasonal to decadal time scales, Atmospheric Chemistry and Physics, 11, 11 221–11 235, https://doi.org/10.5194/acp-11-11221-2011, https://www.atmos-chem-phys.net/11/11221/2011/, 2011.

Wielicki, B. A., Wong, T., Allan, R. P., Slingo, A., Kiehl, J. T., Soden, B. J., Gordon, C. T., Miller, A. J., Yang, S. K., Randall, D. A., Robertson, F., Susskind, J., and Jacobowitz, H.: Evidence for large decadal variability in the tropical mean radiative energy budget. - PubMed - NCBI, Science, 295, 841–844, https://doi.org/10.1126/science.1065837, https://www.ncbi.nlm.nih.gov/pubmed/11823638, 2002.

Winker, D. M. and Osborn, M. T.: Airborne lidar observations of the Pinatubo volcanic plume, Geophysical Research Letters, 19, 167–170, 1992.

https://doi.org/10.5194/acp-2020-344
Preprint. Discussion started: 6 May 2020

Yoshioka, M., Regayre, L. A., Pringle, K. J., Johnson, J. S., Mann, G. W., Partridge, D. G., Sexton, D. M., Lister, G. M., Schutgens, N., Stier, P., Kipling, Z., Bellouin, N., Browse, J., Booth, B. B., Johnson, C. E., Johnson, B., Mollard, J. D., Lee, L., and Carslaw, K. S.: Ensembles of Global Climate Model Variants Designed for the Quantification and Constraint of Uncertainty in Aerosols and Their Radiative Forcing, Journal of Advances in Modeling Earth Systems, 11, 3728–3754, https://doi.org/10.1029/2019MS001628, 2019.

Young, R. E., Houben, H., and Toon, O. B.: Radiatively forced dispersion of the Mt. Pinatubo volcanic cloud and induced temperature perturbations in the stratosphere during the first few months following the eruption, Geophysical Research Letters, 21, 369–372, http://adsabs.harvard.edu/abs/1994GeoRL..21..369Y, 1994.

Young, S. A., Manson, P. J., and Patterson, G. R.: Southern Hemisphere Lidar Measurements of the Aerosol Clouds from Mt. Pinatubo and Mt. Hudson, in: NASA Technical Report, NASA. Langley Research Center, Sixteenth International Laser Radar Conference, Part 1, https://ntrs.nasa.gov/search.jsp?R=19920019987, 1992.

Yu, P., Murphy, D. M., Portmann, R. W., Toon, O. B., Froyd, K. D., Rollins, A. W., Gao, R.-S., and Rosenlof, K. H.: Radiative forcing from anthropogenic sulfur and organic emissions reaching the stratosphere, Geophysical Research Letters, 43, 9361–9367, https://doi.org/10.1002/2016GL070153, http://doi.wiley.com/10.1002/2016GL070153, 2016.

Zanchettin, D., Khodri, M., Timmreck, C., Toohey, M., Schmidt, A., Gerber, E. P., Hegerl, G., Robock, A., Pausata, F. S. R., Ball, W. T., Bauer, S. E., Bekki, S., Dhomse, S. S., LeGrande, A. N., Mann, G. W., Marshall, L., Mills, M., Marchand, M., Niemeier, U., Poulain, V., Rozanov, E., Rubino, A., Stenke, A., Tsigaridis, K., and Tummon, F.: The Model Intercomparison Project on the climatic response to Volcanic forcing (VolMIP): experimental design and forcing input data for CMIP6, Geoscientific Model Development, 9, 2701–2719, https://doi.org/10.5194/GMD-9-2701-2016, 2016.

https://doi.org/10.5194/acp-2020-344
Preprint. Discussion started: 6 May 2020

Atmospheric Chemistry and Physics Discussions

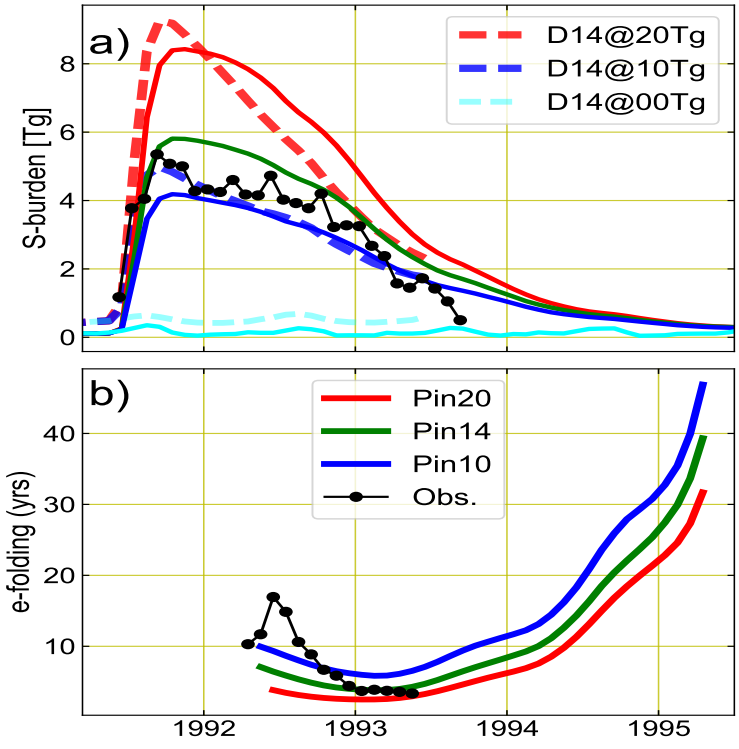

Figure 1. (a, top) Monthly mean stratospheric aerosol (globally integrated above 400 hPa) sulphur burden (S-burden, blue line) from simulations **Pin00**, **Pin10**, **Pin14** and **Pin20**. S-burden from Dhomse et al. (2014) for 0, 10 and 20 Tg SO_2 injection are shown with aqua, red and blue dashed lines, respectively. (b, bottom) Estimated S-burden derived from High-resolution Infrared Radiation Sounder (HIRS) satellite measurements is shown with black dots (Baran and Foot, 1994). (b, lower) S-burden decay rates (e-folding lifetime) calculated using simple linear fit using 6 month S-burden (± 3) time series.

https://doi.org/10.5194/acp-2020-344
Preprint. Discussion started: 6 May 2020

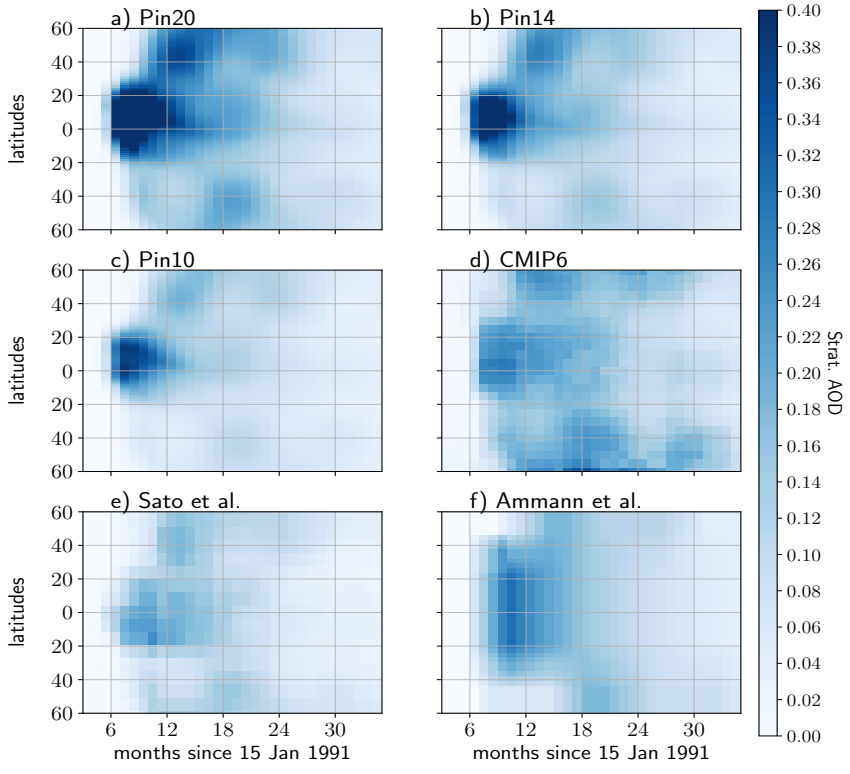

Figure 2. Ensemble mean stratospheric Aerosol Optical Depth (sAOD) from simulations (a) **Pin10**, (b) **Pin14**, and (c) **Pin20**. Panels (d)-(f) show $sAOD_{550}$ from CMIP6, Sato et al. (1993) and Ammann et al. (2003), respectively.

https://doi.org/10.5194/acp-2020-344
Preprint. Discussion started: 6 May 2020

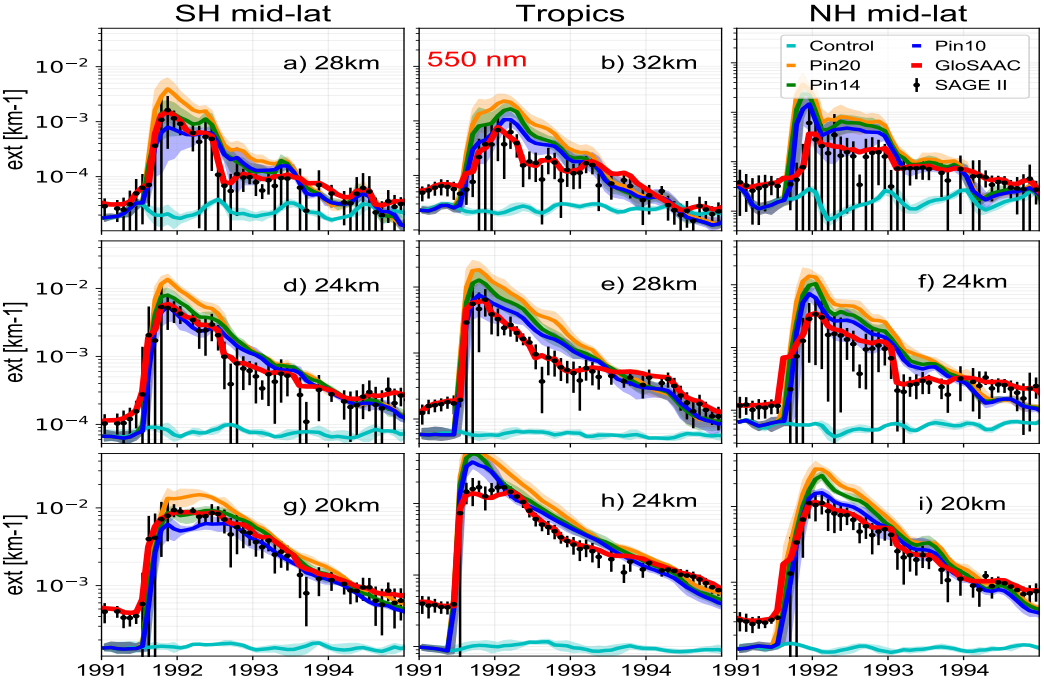

Figure 3. Ensemble mean extinctions (550 nm) from simulations **Pin00** (aqua), **Pin10** (blue), **Pin14** (green), and **Pin20** (orange). The shaded regions indicate the variability among ensemble members. Extinctions for SH mid-latitudes (35°S – 60°S (panels a, d, g)), tropics (20°S – 20°N (panels b, e, h)), and NH mid-latitudes (35°N – 60°N (panels c, f, i)) are shown in left, middle and right panels, respectively. Mid-latitude extinctions are shown for 20, 24 and 28 km, whereas tropical profiles are shown for 24, 28 and 32 km. Monthly mean extinction from SAGE II v7.2 measurements for a given latitude band are shown with black filled circles and vertical lines indicate standard deviation from all the measurements for a given month. Gap-filled extinctions from the GloSSAC dataset (Thomason et al., 2018) are shown with a red line.

https://doi.org/10.5194/acp-2020-344
Preprint. Discussion started: 6 May 2020

Atmospheric Chemistry and Physics Discussions

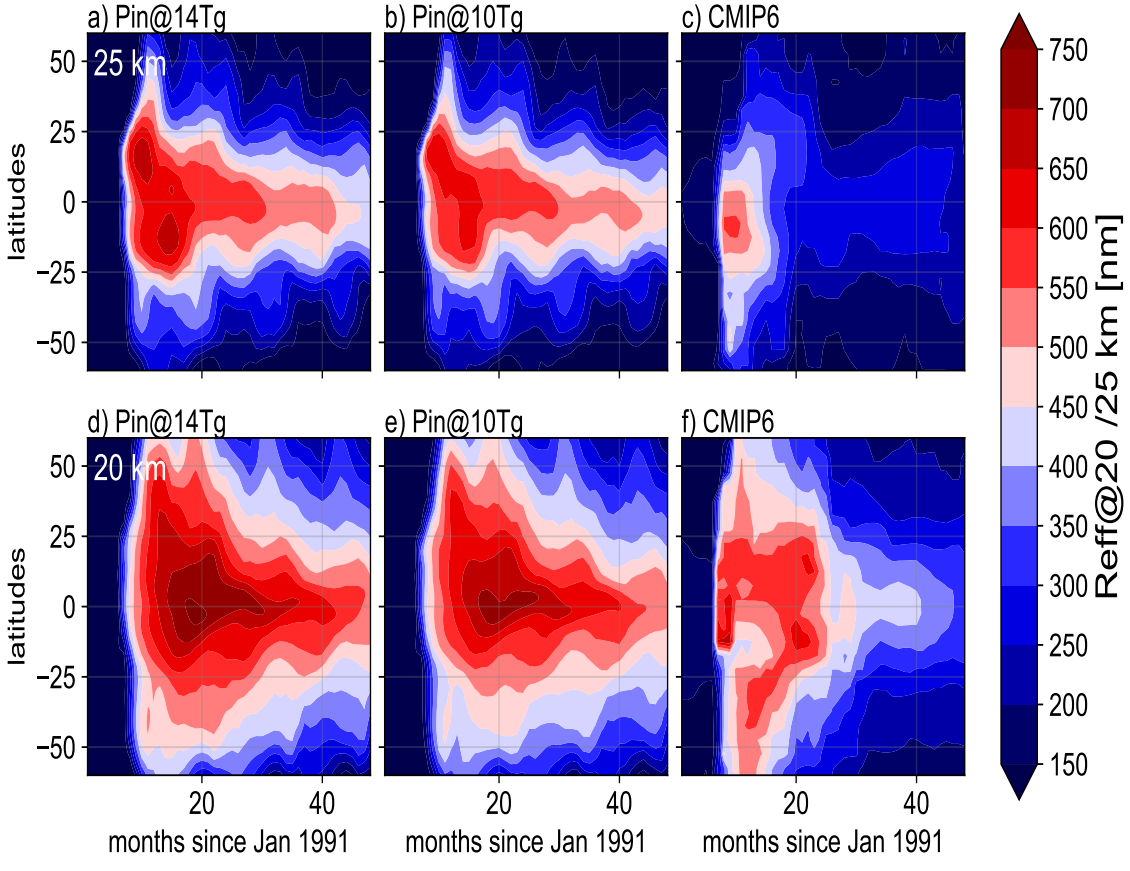

Figure 4. Modelled (from simulations **Pin14** and **Pin20**) and CMIP6 effective radii (Reff, in μm) at (a)-(c) 25 km and (d)-(f) 20 km.

https://doi.org/10.5194/acp-2020-344
Preprint. Discussion started: 6 May 2020

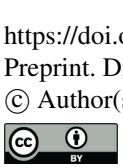

Atmospheric Chemistry and Physics Discussions

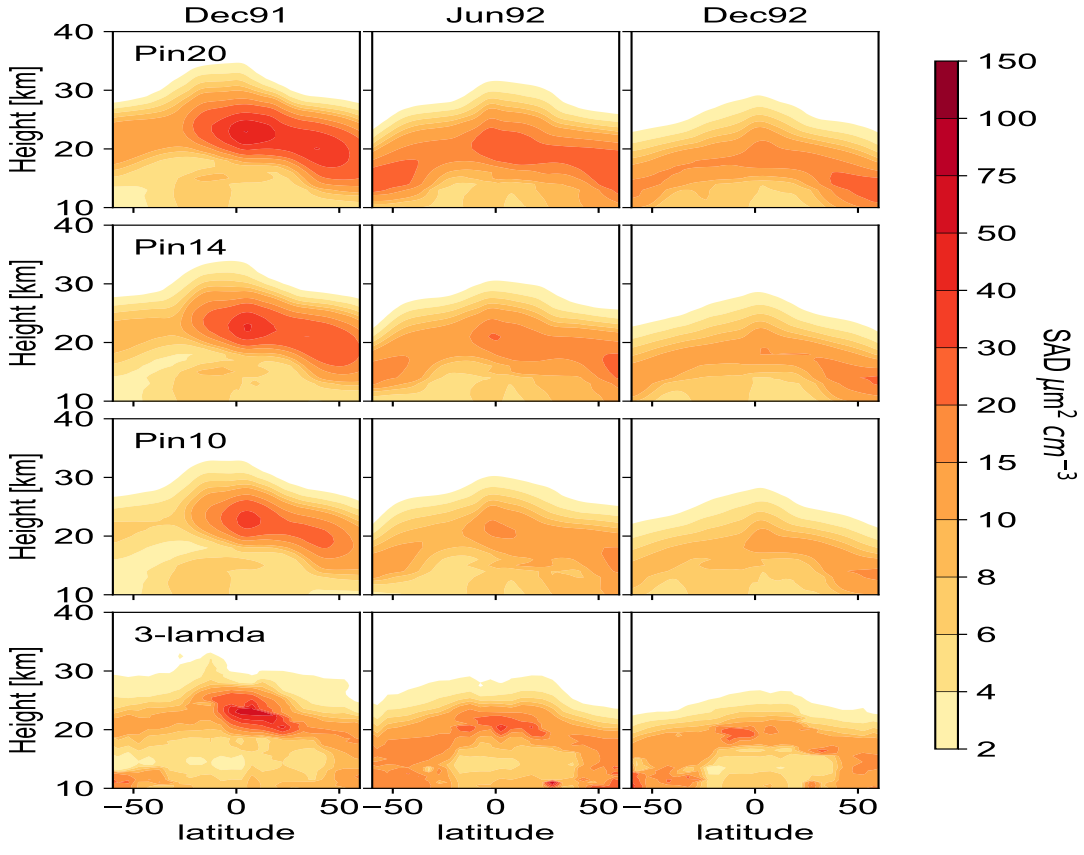

Figure 5. Zonal mean monthly mean Surface Area Density (SAD, μm^2 cm^{-3}) for December 1991, June 1992 and December 1992 from ensemble mean simulations (top row) **Pin20**, (second row) **Pin14**, and (third row) **Pin10**. The bottom row shows observation-based SAD estimates from Arfeuille et al. (2014).

https://doi.org/10.5194/acp-2020-344
Preprint. Discussion started: 6 May 2020

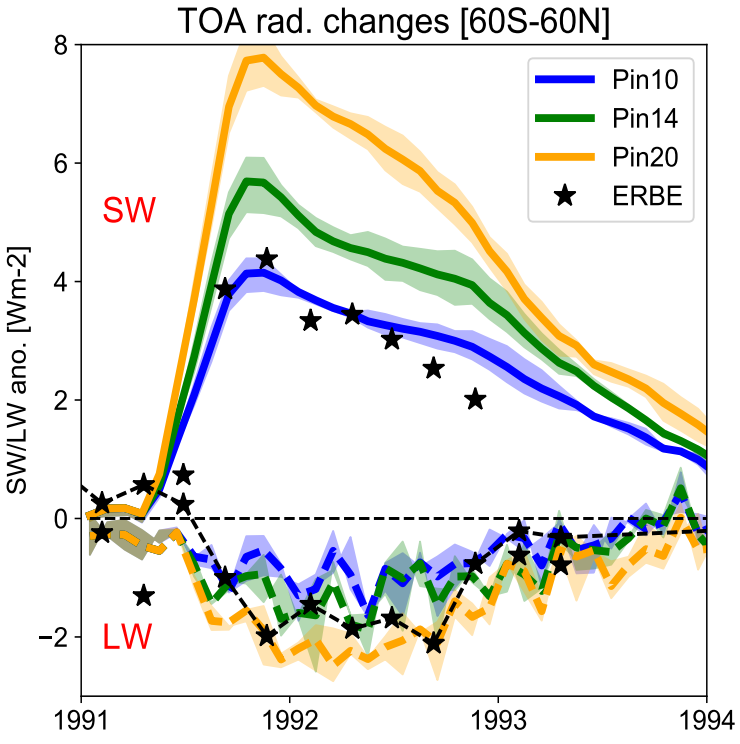

Figure 6. Near-global (60°S-60°N) longwave (LW) and shortwave (SW) heating anomalies (Wm^{-2}) from the ensemble mean of simulations **Pin20** (blue), **Pin14** (green), and **Pin10** (orange). Estimated anomalies from the Earth Radiation Budget Experiment (ERBE) satellite data are shown with black stars.

https://doi.org/10.5194/acp-2020-344
Preprint. Discussion started: 6 May 2020

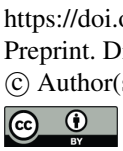

Atmospheric Chemistry and Physics Discussions

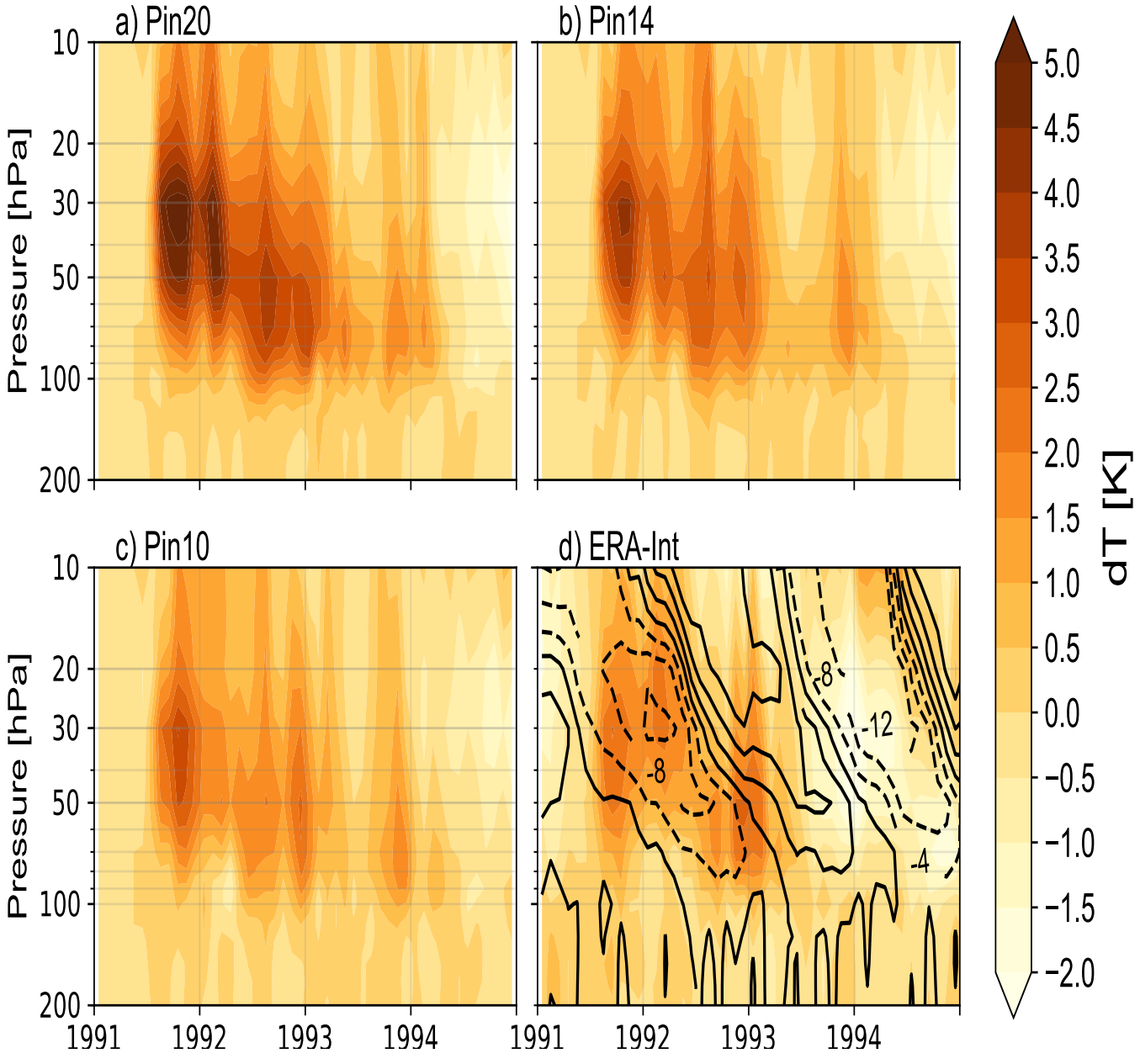

Figure 7. (a)-(c) Ensemble mean aerosol-induced heating (K) in the tropical (20°S – 20°N) stratosphere, calculated by subtracting temperature fields from a control simulation for simulations **Pin20**, **Pin14** and **Pin10**. (d) Tropical temperature (shaded) and zonal wind (contour) anomalies from ERA-Interim reanalysis data (for 1991–1995 time period). Contour intervals for wind anomalies are 4 m/s and negative anomalies are shown with dashed lines.

https://doi.org/10.5194/acp-2020-344
Preprint. Discussion started: 6 May 2020

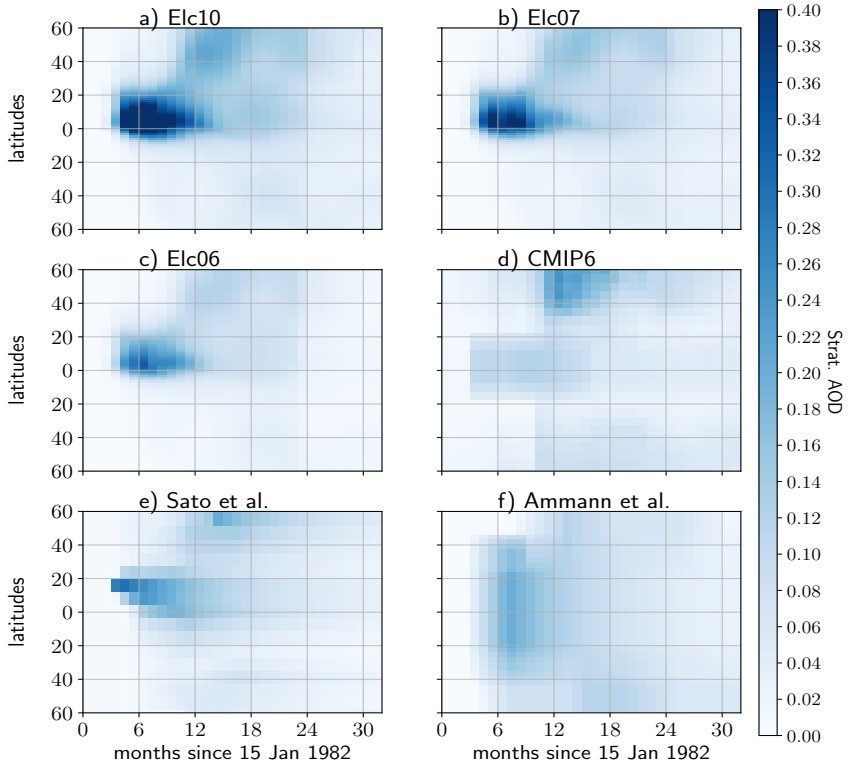

Figure 8. Same as **Fig.** 2, but for El Chichón simulations (a) **Elc10**, (b) **Elc07**, and (c) **Elc05**.

https://doi.org/10.5194/acp-2020-344
Preprint. Discussion started: 6 May 2020

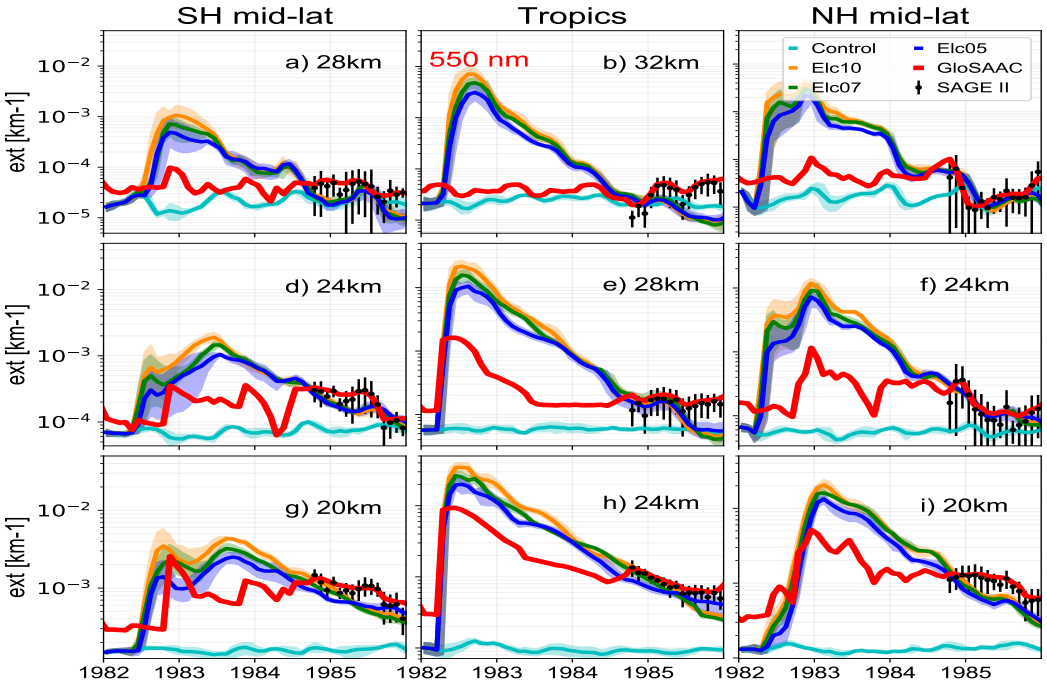

Figure 9. Same as **Fig.** 3, but for El Chichón simulations (a) **Elc05**, (b) **Elc07** and (c) **Elc10**.

https://doi.org/10.5194/acp-2020-344
Preprint. Discussion started: 6 May 2020

Atmospheric Chemistry and Physics Discussions

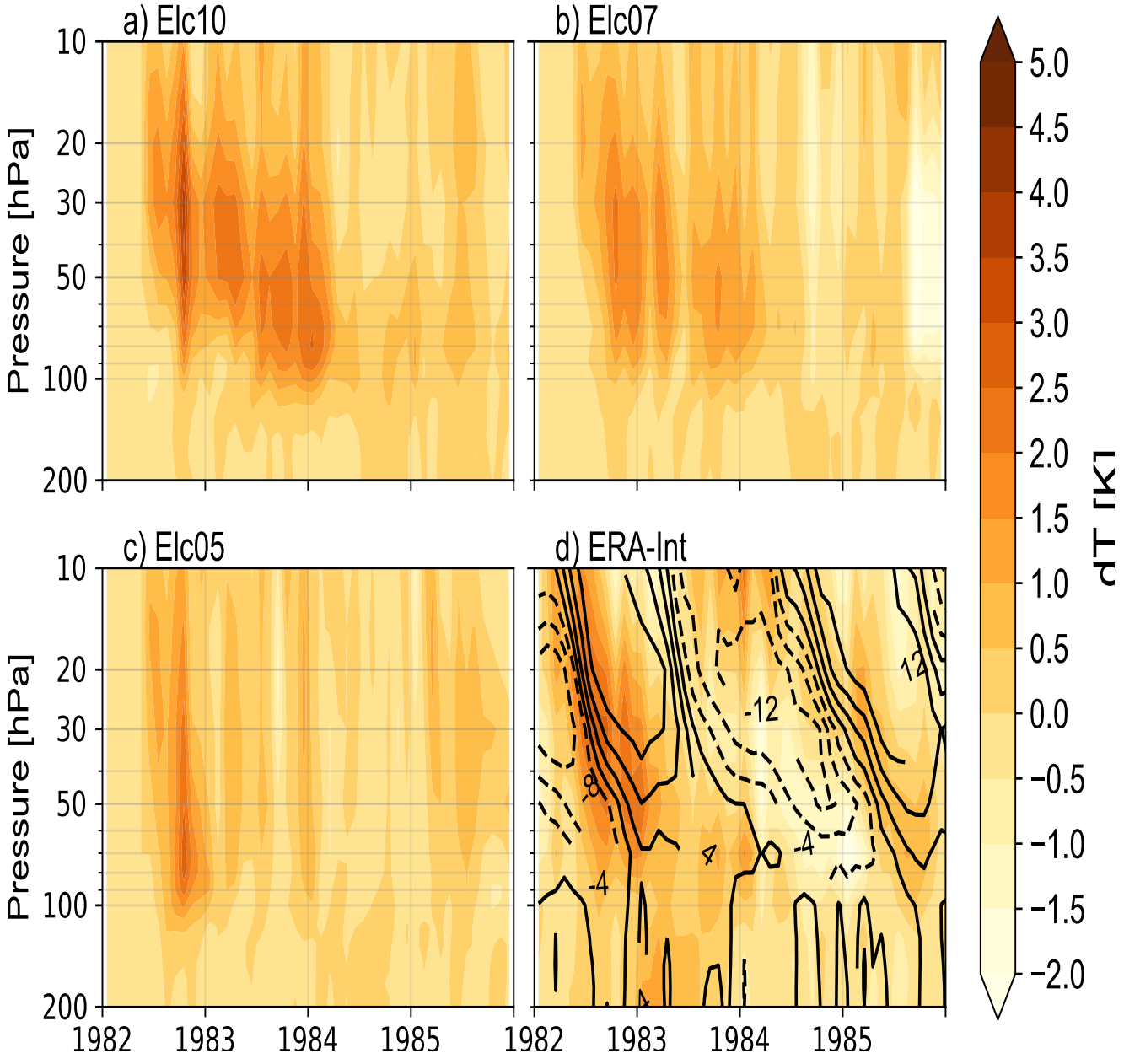

Figure 10. Same as **Fig.** 7, but for El Chichón simulations (a) **Elc10**, (b) **Elc07** and (c) **Elc05**.

https://doi.org/10.5194/acp-2020-344
Preprint. Discussion started: 6 May 2020

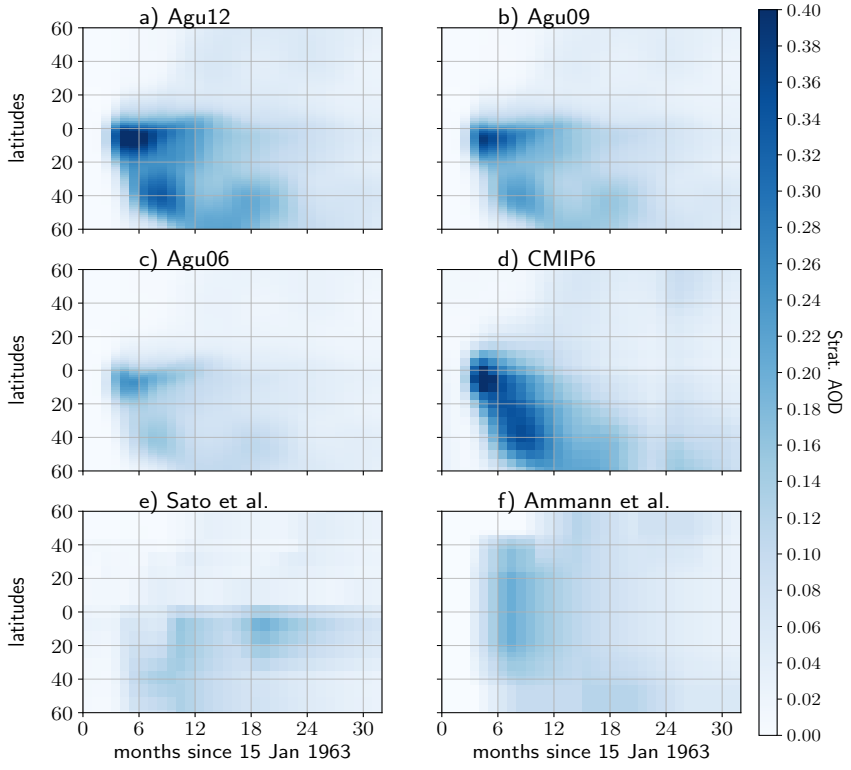

Figure 11. Same as **Fig.** 2, but for Mt. Agung simulations (a) **Agu12**, (b) **Agu09**, and (c) **Agu06**.

https://doi.org/10.5194/acp-2020-344
Preprint. Discussion started: 6 May 2020

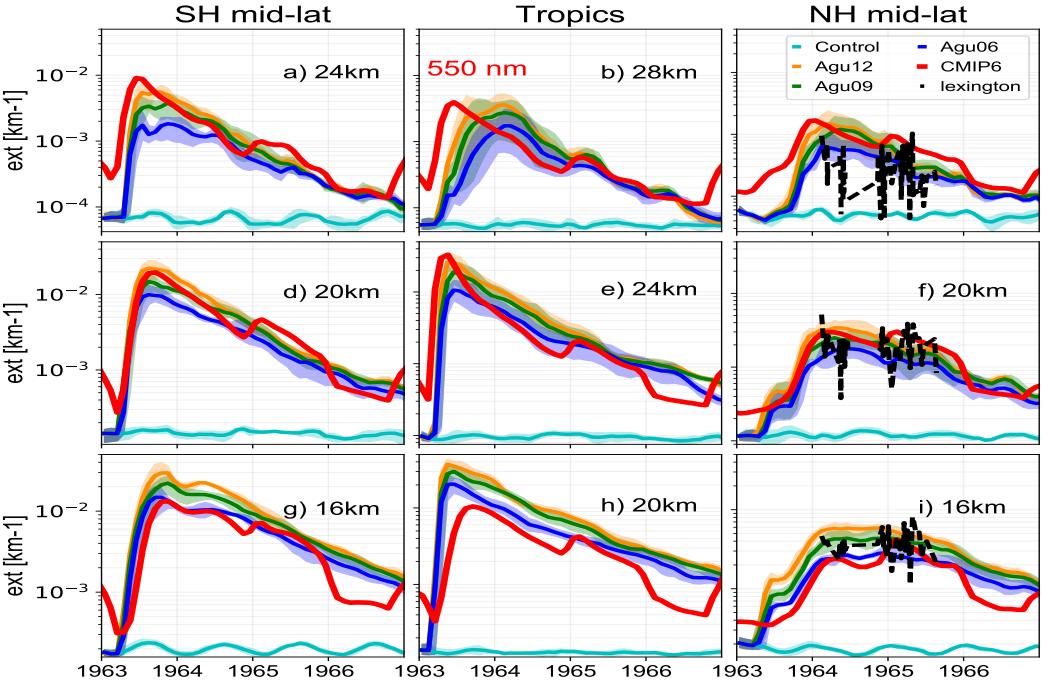

Figure 12. Same as **Fig.** 3, but for Mt. Agung simulations **Agu06**, **Agu09** and **Agu12**. Extinctions are shown for 16, 20 and 24 km for mid-latitudes and 20, 24 and 28 km for the tropics. As GloSSAC data is not available before 1979, model extinctions are compared with CMIP6 data (Arfeuille et al., 2014) and LIDAR measurements from NH mid-latitude station, Lexington, Massachusetts, USA (Grams and Fiocco, 1967)

.

https://doi.org/10.5194/acp-2020-344
Preprint. Discussion started: 6 May 2020

Atmospheric Chemistry and Physics Discussions

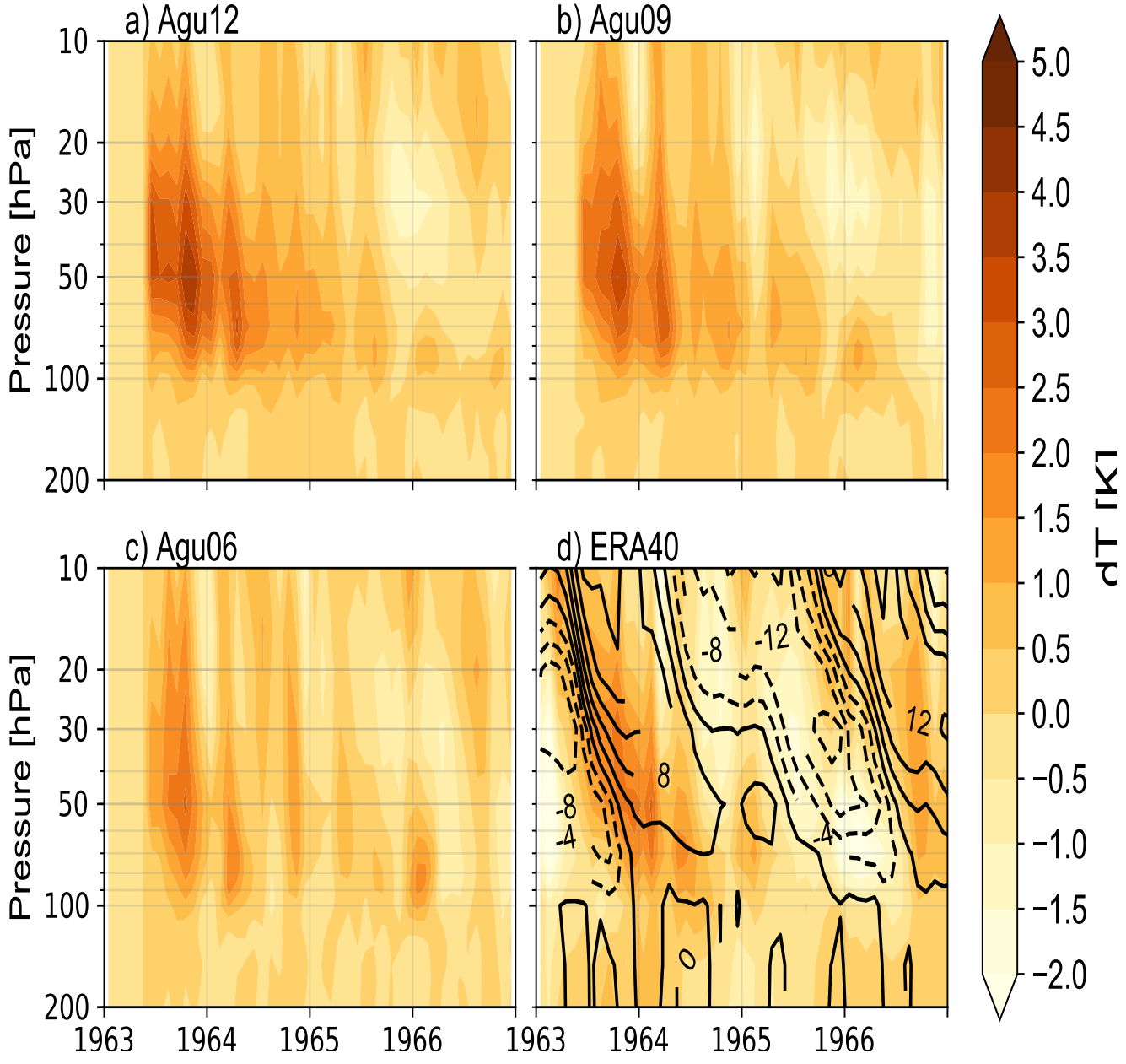

Figure 13. Same as **Fig.** 7, but for Agung simulations (a) **Agu12**, (b) **Agu09** and (c) **Agu06** and for (d) temperature anomalies calculated using ERA-40 reanalysis data.

https://doi.org/10.5194/acp-2020-344
Preprint. Discussion started: 6 May 2020

Atmospheric Chemistry and Physics Discussions

Table 1. Set up of UM-UKCA simulations.

Simulation	Injection amount (Tg SO_2)	Date	Height (km)	QBO phase
Pin00	0	15 June 1991	NA	Easterly
Pin10	10	As **Pin00**	21–23	As **Pin00**
Pin14	14	As **Pin00**	As **Pin10**	As **Pin00**
Pin20	20	As **Pin00**	As **Pin10**	As **Pin00**
Elc00	0	4 April 1982	NA	Westerly
Elc05	5	As **Elc00**	24–26	As **Elc00**
Elc07	7	As **Elc00**	As **Elc05**	As **Elc00**
Elc10	10	As **Elc00**	As **Elc05**	As **Elc00**
Agu00	0	17 March 1963	NA	Westerly
Agu06	6	As **Agu00**	20–22	As **Agu00**
Agu09	9	As **Agu00**	As **Agu06**	As **Agu00**
Agu12	12	As **Agu00**	As **Agu06**	As **Agu00**